

Paleoceanography and Paleoclimatology

RESEARCH ARTICLE

10.1029/2022PA004418

Special Section:

DeepMIP in the Hothouse Earth: Late Paleocene-Early Eocene Climates and Their Lessons for the Future

Key Points:

- Early Eocene southern Australia average temperatures were over 5°C warmer than today, despite being further south than today
- Average rainfall was much higher than today, with 60 cm yr⁻¹ inland to >100 cm yr⁻¹ closer to the coast
- Southern Australia was more homogeneously green and productive during the Eocene, in places where today arid shrub- and grasslands dominate

Correspondence to:

T. Reichgelt and D. R. Greenwood,
tammo.reichgelt@uconn.edu;
greenwood@brandonu.ca

Citation:

Reichgelt, T., Greenwood, D. R., Steinig, S., Conran, J. G., Hutchinson, D. K., Lunt, D. J., et al. (2022). Plant proxy evidence for high rainfall and productivity in the Eocene of Australia. *Paleoceanography and Paleoclimatology*, 37, e2022PA004418. <https://doi.org/10.1029/2022PA004418>

Received 19 JAN 2022

Accepted 4 MAY 2022

Author Contributions:

Conceptualization: Tammo Reichgelt, David R. Greenwood, John G. Conran, Daniel J. Lunt








Data curation: Tammo Reichgelt, David R. Greenwood, Sebastian Steinig, John G. Conran, David K. Hutchinson, Leonie J. Scriven, Jiang Zhu

Formal analysis: Tammo Reichgelt, David R. Greenwood

Funding acquisition: David R. Greenwood, John G. Conran, David K. Hutchinson, Daniel J. Lunt

Investigation: Tammo Reichgelt, David R. Greenwood, Sebastian Steinig, John G. Conran, David K. Hutchinson, Leonie J. Scriven, Jiang Zhu

Plant Proxy Evidence for High Rainfall and Productivity in the Eocene of Australia

Tammo Reichgelt¹ , David R. Greenwood² , Sebastian Steinig³ , John G. Conran⁴ , David K. Hutchinson⁵ , Daniel J. Lunt³ , Leonie J. Scriven⁶, and Jiang Zhu⁷ 

¹Department of Geosciences, University of Connecticut, Mansfield, CT, USA, ²Department of Biology, Brandon University, Brandon, MB, Canada, ³School of Geographical Sciences, University of Bristol, Bristol, UK, ⁴ACEBB & SGC, School of Biological Sciences, The University of Adelaide, Adelaide, SA, Australia, ⁵Climate Change Research Centre, University of New South Wales, Sydney, NSW, Australia, ⁶Botanic Gardens and State Herbarium, Adelaide, SA, Australia, ⁷Climate and Global Dynamics Laboratory, National Center for Atmospheric Research, Boulder, CO, USA

Abstract During the early to middle Eocene, a mid-to-high latitudinal position and enhanced hydrological cycle in Australia would have contributed to a wetter and “greener” Australian continent where today arid to semi-arid climates dominate. Here, we revisit 12 southern Australian plant megafossil sites from the early to middle Eocene to generate temperature, precipitation, and seasonality paleoclimate estimates, net primary productivity (NPP), and vegetation type, based on paleobotanical proxies and compare them to early Eocene global climate models. Temperature reconstructions are uniformly subtropical (mean annual, summer, and winter mean temperatures 19–21°C, 25–27°C, and 14–16°C, respectively), indicating that southern Australia was ~5°C warmer than today, despite a >20° poleward shift from its modern geographic location. Precipitation was less homogeneous than temperature, with mean annual precipitation of ~60 cm over inland sites and >100 cm over coastal sites. Precipitation may have been seasonal with the driest month receiving 2–7× less than the mean monthly precipitation. Proxy-model comparison is favorable with a 1,680 ppm CO₂ concentration. However, individual proxy reconstructions can disagree with models as well as with each other. In particular, seasonality reconstructions have systemic offsets. NPP estimates were higher than modern, implying a more homogeneously “green” southern Australia in the early to middle Eocene when this part of Australia was at 48–64°S and larger carbon fluxes to and from the Australian biosphere. The most similar modern vegetation type is modern-day eastern Australian subtropical forest, although the distance from coast and latitude may have led to vegetation heterogeneity.

Plain Language Summary Australia today is dominated by arid environments, with sparse shrubland or grassland vegetation, and forest biomes limited to areas with abundant moisture supply. These arid environments have low primary productivity and store relatively little carbon. Examination of 12 early to middle Eocene (55–40 million years old) fossil floras shows that southern Australia at that time was much “greener.” In a globally warmer world and poleward positioning of southern Australia, southward of mid-latitude high-pressure systems, rainfall in now arid environments was much higher. What is now almost barren landscapes would have supported a much more luxurious forested biome. As a result, primary productivity was enhanced and on-land carbon storage would have been much higher as well. This research shows that in ancient greenhouse worlds high temperatures in addition to a more active hydrological cycle can lead to an increase in carbon storage and fluxes of the terrestrial biosphere.

1. Introduction

The early to middle Eocene experienced the highest average global temperatures of the Cenozoic and since then, temperatures have in general steadily declined from global hothouse conditions to an icehouse (e.g., Westerhold et al., 2020). Proxy and model reconstructions for the early to middle Eocene still commonly produce a wide range of possible temperatures in tropical latitudes and reconstructed atmospheric carbon dioxide concentrations at this time are widely variable (Beerling & Royer, 2011; Foster et al., 2017; Lunt et al., 2021; Shukla et al., 2014; Spicer et al., 2014). However, proxy and model reconstructions are in agreement that the early to middle Eocene Arctic and the Antarctic were ice-free and vegetated (e.g., Contreras et al., 2013; Eberle & Greenwood, 2012; Pross et al., 2012; West et al., 2020), and that a shallower than Holocene poles-to-tropics temperature gradient existed in both sea surface and terrestrial temperatures (Bijl et al., 2009; Greenwood & Wing, 1995; Ho &

Methodology: Tammo Reichgelt, Sebastian Steinig
Project Administration: Tammo Reichgelt, David R. Greenwood
Supervision: Tammo Reichgelt, David R. Greenwood
Validation: Tammo Reichgelt, David R. Greenwood, Daniel J. Lunt
Visualization: Tammo Reichgelt, David R. Greenwood, Sebastian Steinig
Writing – original draft: Tammo Reichgelt, David R. Greenwood, John G. Conran
Writing – review & editing: Tammo Reichgelt, David R. Greenwood, John G. Conran, David K. Hutchinson, Daniel J. Lunt, Jiang Zhu

Laepple, 2016; Huber & Caballero, 2011; J. Zhu et al., 2019). A “supercharged” hydrological cycle likely accompanied the globally elevated temperatures (Carmichael et al., 2016), like tropical storms and atmospheric rivers transported moisture from the tropics to higher latitudes (Kiehl et al., 2021; Shields et al., 2021) and increased extreme precipitation events (Carmichael et al., 2016).

During the early to middle Eocene, Australia was located between 35 and 65°S (Figure 1; see also Greenwood & Christophel [2005]). The extent of the Australian continental landmass was relatively stable over the Cenozoic and likely had a similar area as it has today (~7.5 million km²), although a large inland basin, the Lake Eyre Basin (1.1 million km²), was likely flooded at least partially during this time and a succession of marine transgressions flooded low-lying parts of the southern margin of the continent (Alley, 1998; Benbow et al., 1995; Habeck-Fardy & Nanson, 2014). As such, it represents the largest continental area in southern mid-to-high latitudes during the Paleogene. However, few quantitative paleoclimate reconstructions exist for Eocene Australia that could provide crucial data on the Southern Hemisphere Eocene tropical to polar latitudinal temperature gradient (e.g., Greenwood & Wing, 1995), or the capacity of rain to reach the continental interior of a large Southern Hemisphere landmass with a supercharged Eocene hydrological cycle. Today, most of the Australian continent (~5 million km²) has an arid to semi-arid climate (rainfall/evaporation <0.4 and mean annual precipitation <40 cm yr⁻¹) supporting sparse vegetation with forest cover largely restricted to the wetter coastal areas (Morton et al., 2011). However, paleobotanical data have demonstrated that Australian vegetation in the Eocene was very different from today (e.g., Christophel & Greenwood, 1989; Greenwood, 1996; Greenwood & Christophel, 2005; Greenwood et al., 2017), consistent with the idea of a supercharged hydrological cycle projecting wet airmasses into the interior.

Plants interact directly with their environment, taking on a typical physiognomy and having strict distribution limits in response to the macroclimate (e.g., Chen et al., 2011; Lusk et al., 2018; Punyasena, 2008; Reichgelt et al., 2018; Wright et al., 2017; Yang et al., 2015). Additionally, biomes are shaped principally by climate and are characterized by the life-forms and taxonomic groups of plants they contain, as plants are the main primary producers in most ecosystems (Beer et al., 2010; Whittaker, 1962) and by far exceed any other type of organism in sheer biomass (Bar-On et al., 2018). As such, plant fossils are valuable indicators of terrestrial paleoclimate and paleoecology (Peppe et al., 2018). Paleobotanical proxies for ancient climates have been applied widely to Eocene paleofloras, especially in the northern temperate and Arctic regions (e.g., Spicer et al., 2016; Teodoridis et al., 2012; West et al., 2020). In the Southern Hemisphere, early Eocene terrestrial temperatures have been reconstructed for South America (Gayó et al., 2005; Hinojosa, 2005; Hyland et al., 2017; Wilf et al., 2005), New Zealand (Pancost et al., 2013), Antarctica (Bijl et al., 2013; Pross et al., 2012), and Australia (Carpenter et al., 2012; Greenwood et al., 2003; Huurdeman et al., 2021; Pole, 2019), showing early Eocene southern mid-to-high latitude mean annual temperatures to be 5–15°C higher than today, with a shallower equator-to-pole temperature gradient (Greenwood & Wing, 1995; Naafs et al., 2018). However, few paleoprecipitation reconstructions exist for the southern mid-to-high latitudes (e.g., Greenwood, 1996; Greenwood et al., 2017, 2003; Huurdeman et al., 2021; Pole, 2019; Pross et al., 2012; Wilf et al., 2005) and attempts to link vegetation, paleoclimate and paleoproductivity are non-existent.

Here, we present a comprehensive analysis of early to middle Eocene paleoclimate and vegetation from 12 southern Australian fossil floras. We combine multiple floral paleoclimate proxies, calibrated with modern leaf physiognomy or species distribution, and generate a single ensemble estimate for each paleoclimate parameter for each site (Greenwood et al., 2017; Lowe et al., 2018; West et al., 2020). The reconstructed temperature, precipitation, and seasonality were then compared to modeled climate extracted from paleo-coordinates corresponding to the locations where the fossil floras were deposited using early to middle Eocene global climate models (Hutchinson et al., 2018; J. Zhu et al., 2019). A novel method to reconstruct vegetation productivity in the Southern Hemisphere is also used here. The vegetation type is reconstructed in relation to leaf physiognomy and the reconstructed paleoclimate, in order to estimate the coast-to-continental interior vegetation transition and the associated changes in productivity during the early to middle Eocene.

2. Methods

2.1. Australian Eocene Floras

The 12 floras studied here span from southern Queensland in the east of Australia to Tasmania in the south, and Western Australia in the west (Table 1, Figure 1). The modern latitudes of these megaflores sites span 28–42°S,

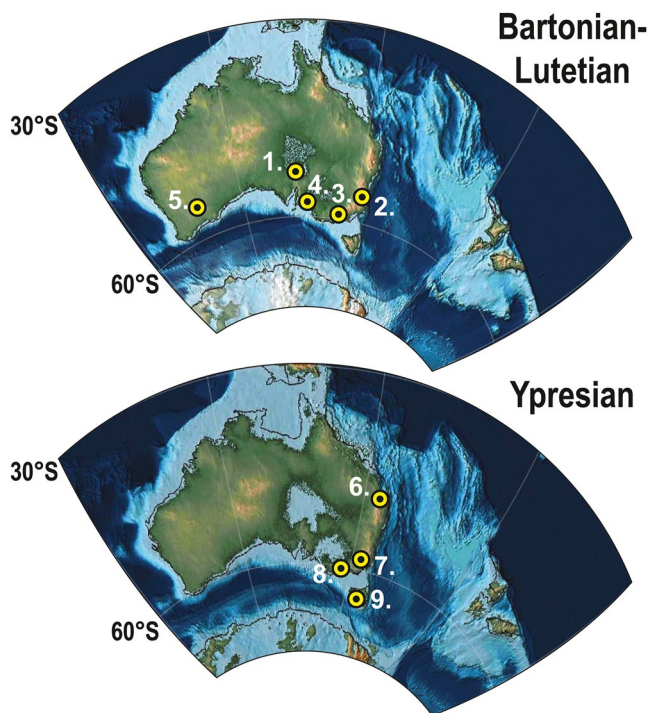


Figure 1. Paleogeography of Australia during the Ypresian (early) and Lutetian/Bartonian (middle) stages of the Eocene (Scotese, 2016), with locations of study sites (Table 1): 1. Poole Creek & Nelly Creek, 2. Nerriga, 3. Anglesea, 4: Golden Grove & Maslin Bay, 5: Lefroy & Cowran, 6. Dinmore, 7. Brandy Creek & Hotham Heights, 8. Deans Marsh, 9. Regatta Point.

but because of the substantial Cenozoic northward movement of the Australian continent, the paleolatitudes at the time of deposition of the floras span 48–64°S (Table 1, Figure 1). Currently, the only landmasses at these latitudes are the southernmost part of South America, including Tierra del Fuego, the Falkland Islands, and the northern tip of the Antarctic Peninsula. Eight sites were subjected to four paleobotanical proxies: the Climate Leaf Analysis Multivariate Program (CLAMP) (Spicer et al., 2021; Wolfe, 1993; Yang et al., 2015), Leaf Area Analysis (LAA) (Peppe et al., 2011; Wilf et al., 1998), Leaf Margin Analysis (LMA) (Greenwood et al., 2004; Peppe et al., 2011; Wilf, 1997) and Nearest Living Relative analysis (NLR) (Greenwood et al., 2003; Grimm & Potts, 2016; Kershaw, 1997). A more comprehensive explanation of these proxies is given in Sections 2.2 and 2.3. These eight sites are Poole Creek, Nelly Creek, Deans Marsh, Nerriga, Golden Grove, Maslin Bay, Anglesea, and Dinmore. These sites could be subjected to these paleobotanical paleoclimate proxies because, first, the quality of preservation at these sites allowed for measurements needed for physiognomic proxies, and second, prior work had established taxonomic affinities of floral elements to modern plant groups. For Brandy Creek and Hotham Heights only LMA and NLR were performed, since these megaflores were not complete enough to determine leaf sizes (Greenwood et al., 2017) and for Regatta Point and Lefroy & Cowran, only NLR was used since these floras represent dispersed cuticle for which neither the leaf margin architecture nor leaf sizes could be determined (Carpenter & Pole, 1995; Pole, 2007). For all sites, the proxies are based on megafossils (leaves, fruits, flowers) and not on plant spores and pollen, in order to obtain a local paleoclimate signal and prevent overprinting by a regional signal.

Previous accounts of some of these floras—Anglesea, Deans Marsh, Golden Grove, Maslin Bay, Nelly Creek, Nerriga, and Poole Creek—presented an either qualitative analysis of the leaf physiognomy or used a limited set of

modern calibrations (e.g., Christophel & Greenwood, 1989; Greenwood, 1994, 1996; Greenwood et al., 2003); however, here we re-analyze the original quantitative leaf physiognomic data of these works using a wide set of calibrations including CLAMP. Two inland floras studied here are Poole Creek and Nelly Creek (Table 1), part of the Eyre Formation (Alley et al., 1996; Greenwood, 1996). Both floras are regarded as middle Eocene (Lutetian – Bartonian), based on palynological zonation (Alley et al., 1996; Rozefelds et al., 2021). Leaf physiognomic measurements presented here for Poole and Nelly Creek are derived and refined from data collected in earlier studies (Christophel et al., 1992; Greenwood, 1994, 1996). Prior paleobotanical studies established the taxonomic affinities of plant megafossils at Poole and Nelly Creek (Conran et al., 2003; Greenwood, 1996; Greenwood & Christophel, 2005; Rozefelds et al., 2021; Vadala & Greenwood, 2001).

Two floras from the Eastern View Formation in southern Victoria are analyzed here—the early Eocene (Ypresian) Deans Marsh flora and middle Eocene (Bartonian to basal Priabonian) Anglesea flora (Table 1, Figure 1). Both floras were dated using palynological zonation (Greenwood et al. [2003] and references cited therein). Leaf physiognomic data used here was derived and refined from data collected in earlier studies (Christophel et al., 1987; Christophel & Greenwood, 1989; Greenwood, 1994; Greenwood et al., 2003). Taxonomic affinities of plant megafossils at Deans Marsh and Anglesea were derived from earlier paleobotanical studies (Christophel et al., 1987; Greenwood, 1987; Greenwood & Christophel, 2005; Greenwood et al., 2003; Vadala & Greenwood, 2001).

The Nerriga flora is found in the Titringo siltstone in southeastern New South Wales (Table 1, Figure 1) and was dated at 42.6–45.9 million years old (middle Eocene, Lutetian) based on K-Ar dating (Hill, 1982). Leaf physiognomic data used here were derived and refined from data collected previously (Hill, 1982, 1986). Taxonomic affinities of megafossils from Nerriga were derived from earlier paleobotanical work (Conran & Christophel, 1998; Greenwood & Christophel, 2005; Greenwood et al., 2003; Hill, 1982, 1986; Vadala & Greenwood, 2001).

Table 1
Summary of Site Information of Early to Middle Eocene Australian Paleofloras

Site name	Lat/long (°S, °E)	Paleo-lat/long (°S, °E)	Age	Formation	Available proxies	(Morpho)-taxa
Poole Creek	29.6, 137.7	50.7, 130.9	Lutetian – Bartonian ^b	Eyre Fm	CLAMP ^a , LAA ^a , LMA ^a , NLR ^{b,i}	14, 14, 14, 14
Nelly Creek	29.3, 137.7	50.4, 130.8	Lutetian – Bartonian ^b	Eyre Fm	CLAMP ^a , LAA ^a , LMA ^a , NLR ^{i,j,k}	14, 14, 14, 9
Deans Marsh	38.4, 143.9	60.7, 145.7	Ypresian ^c	Eastern View	CLAMP ^a , LAA ^a , LMA ^a , NLR ^c	18, 18, 18, 10
Nerriga	35.1, 150.1	54.2, 149.5	42.6–45.9 MYA (Lutetian) ^d	Titringo siltstone	CLAMP ^a , LAA ^a , LMA ^a , NLR ^{c,d,k,l}	25, 24, 24, 15
Golden Grove	34.8, 138.7	55.7, 133.5	Lutetian ^e	North Maslin Sands	CLAMP ^a , LAA ^a , LMA ^a , NLR ^{c,m,n,o}	21, 21, 21, 19
Maslin Bay	35.2, 138.5	56.2, 133.2	Lutetian ^e	North Maslin Sands	CLAMP ^a , LAA ^a , LMA ^a , NLR ^{k,p,q,r}	120, 120, 120, 29
Anglesea	38.4, 144.2	58.1, 141.6	Bartonian ^c	Eastern View	CLAMP ^a , LAA ^a , LMA ^a , NLR ^{c,k,s,t}	28, 27, 27, 24
Dinmore	27.6, 152.8	48.2, 153.2	Ypresian ^f	Redbank Plains	CLAMP ^f , LAA ^f , LMA ^f , NLR ^{f,u}	20, 20, 20, 12
Brandy Creek	37.0, 147.3	58.6, 150.1	Ypresian – Bartonian ^v	Mt Jim Volc Group	LMA ^v , NLR ^v	18, 20
Hotham Heights	37.0, 147.2	58.6, 149.9	Ypresian – Bartonian ^v	Mt Jim Volc Group	LMA ^v , NLR ^v	26, 24
Regatta Point	42.2, 145.3	64.0, 150.3	Ypresian ^g	-	NLR ^{g,w,x}	21
Lefroy & Cowran	31.2, 121.7	52.1, 108.2	Bartonian ^h	Werillup-Pidinga	NLR ^y	18

Note. Available proxies represent the paleobotanical climate proxies that we used in this study for these sites: CLAMP—Climate Leaf Analysis Multivariate Program (Kennedy et al., 2014; Wolfe, 1993), LAA—Leaf Area Analysis (Wilf et al., 1998), LMA—Leaf Margin Analysis (Greenwood et al., 2004; Peppe et al., 2011; Wilf, 1997) and NLR—Nearest Living Relative analysis (West et al., 2020; Willard et al., 2019). Number of morphotaxa or taxa used differs per proxy because CLAMP, LAA and LMA do not rely on taxonomic assignments, but morphotaxa may have key characteristics missing, and NLR does rely on taxonomic assignments and includes non-angiosperms. All morphological and physiognomic data on which analyses are based are presented in Supporting Tables S1–6.

^aNew data this study. ^bRozefelds et al., 2021. ^cGreenwood et al., 2003. ^dHill, 1982. ^eScriven et al., 1995. ^fPole, 2019. ^gPole & Macphail, 1996. ^hClarke, 1994. ⁱGreenwood, 1996. ^jConran et al., 2003. ^kVadala and Greenwood, 2001. ^lConran and Christophel, 1998. ^mChristophel and Greenwood, 2004. ⁿBasinger et al., 2007. ^oChristophel and Greenwood, 1987. ^pCarpenter et al., 2006. ^qChristophel and Blackburn, 1978. ^rBarnes and Hill, 1999. ^sChristophel et al., 1987. ^tGreenwood, 1987. ^uRozefelds et al., 2016. ^vGreenwood et al., 2017. ^wPole, 2007. ^xConran et al., 2009. ^yCarpenter and Pole, 1995.

The Golden Grove and Maslin Bay floras were collected from quarries intersecting the North Maslin Sands, near Adelaide in South Australia (Table 1, Figure 1). Based on palynological zonation, both floras are considered middle Eocene (Lutetian) (Greenwood & Christophel, 2005; Greenwood et al., 2003; Scriven et al., 1995). Leaf physiognomic data used here were derived and refined from data collected previously (Carpenter et al., 2006; Christophel & Greenwood, 1987; Greenwood, 1996; Greenwood & Christophel, 2005; Greenwood et al., 2003; Scriven, 1993; Scriven et al., 1995; Scriven & Hill, 1995). The taxonomic affinities of plant megafossils from Golden Grove and Maslin Bay were derived from earlier paleobotanical studies (Barnes & Hill, 1999; Basinger et al., 2007; Carpenter et al., 2006; Christophel & Blackburn, 1978; Christophel & Greenwood, 1987; Conran & Christophel, 2004; Greenwood & Christophel, 2005; Greenwood et al., 2003; Vadala & Greenwood, 2001).

The Hotham Heights and Brandy Creek floras were deposited relatively close to each other, in the alpine area of central Victoria (Table 1, Figure 1). These floras are part of fluvial deposits capped by basalts of the Mount Jim Volcanic Group and were dated as early to middle Eocene (Ypresian – Lutetian), or latest middle Eocene (Bartonian) based on palynological zonation (Greenwood et al., 2003, 2017; Holdgate et al., 2008). Both the leaf physiognomy (leaf margin only) and taxonomic affinities of these two floras are based on previous paleobotanical work (Carpenter et al., 2004; Greenwood et al., 2017).

The Dinmore flora was deposited in the southeastern Queensland Redbank Field Formation (Table 1, Figure 1). The flora is dated as early Eocene (Ypresian) based on lithostratigraphic correlations and palynological zonation (Pole, 2019). Leaf physiognomy and taxonomic affinities of the flora were both described by Pole (2019).

The Regatta Point flora is the southernmost flora considered here, in Tasmania (Table 1, Figure 1). The Regatta Point beds are considered early Eocene (Ypresian) based on palynological zonation (Pole & Macphail, 1996). The site is known for the southernmost occurrence of the tropical mangrove palm *Nypa* (Pole & Macphail, 1996). Taxonomic affinities at Regatta Point are based on cuticles from prior paleobotanical studies (Conran et al., 2009; Pole, 2007; Pole & Macphail, 1996). Prior analysis of the paleoclimate from the Regatta Point flora using NLR and a novel proxy based on *Podocarpus* leaf size inferred near-tropical temperatures (Carpenter et al., 2012).

The Cowran and Lefroy paleodrainages floras represent dispersed cuticles recovered from several cores within the Werillup and Pidinga Formations in Western Australia (Table 1, Figure 1). Though this flora represents multiple cores in different locations, the formations were part of the same Eocene paleodrainage (Clarke, 1994) and were placed in the late-middle Eocene (Bartonian) using palynological zonation (Carpenter & Pole, 1995). Affinities of the cuticle recovered from the Cowran and Lefroy paleodrainages are based on the identifications of Carpenter and Pole (1995).

2.2. Leaf Physiognomy as a Climate Proxy

Leaf physiognomy is highly responsive to macroclimate, largely independent of taxonomy (e.g., Lusk et al., 2018; Wright et al., 2017; Yang et al., 2015). As such, fossil leaf physiognomy can be employed to estimate terrestrial paleoclimate (Peppe et al., 2018; Spicer et al., 2021; Wilf et al., 1998). Correlations between leaf traits and climate in modern leaf assemblages can constrain paleoclimate based on similarities and dissimilarities to the fossil megafloora leaf traits. These correlations can either be based on single or multiple leaf parameters to constrain paleoclimate, using univariate or multivariate analyses, respectively.

2.2.1. Climate Leaf Analysis Multivariate Program

CLAMP is a multivariate terrestrial paleoclimate proxy based on categorized leaf traits derived from fossil leaves (Spicer et al., 2021; Wolfe, 1993). Dimension reduction using Canonical Correspondence Analysis (CCA) is applied to the categorized leaf traits together with a modern-day leaf calibration dataset, for which the traits have been similarly categorized, but of which the climate is known. The categorized leaf traits used here are leaf margin type (three categories), leaf area (seven categories), leaf apex shape (four categories), leaf base shape (three categories), and leaf length to width ratio (five categories). The environmental variables included in CCA here were mean annual temperature (MAT), mean diurnal range (MDR), warmest and coldest quarter mean temperature (WQT and CQT), mean annual precipitation (MAP), wettest and driest month precipitation (WMP and DMP) and net primary productivity (NPP). MAT, MDR, WQT, CQT, WMP, and DMP were derived from WORLDCLIM (Fick & Hijmans, 2017) and NPP were derived from MODIS (Running et al., 2015). The modern-day calibration leaf physiognomy dataset used here (Supporting Information Table S1) is a Southern Hemisphere-based dataset (Kennedy et al., 2014), supplemented with sites from Chile (Hinjosa et al., 2006) and southeastern Australia (Reichgelt et al., 2019).

Site scores for each modern-day calibration and fossil leaf assemblage are generated for $n = 4$ CCA axes using the `cca` and `predict.cca` functions of the `vegan` package in R (Oskanen et al., 2019). Then, site vectors scores (V) in four CCA dimensions between site physiognomy (CCA_p) and each environmental (CCA_e) variable can be calculated.

$$V = \frac{\sum_{i=1}^4 CCA_e \times CCA_p}{\sum_{i=1}^4 \sqrt{CCA_e^2}} \quad (1)$$

Quadratic polynomial regression functions are then established between site V -scores and MAT, MDR, WQT, CQT, WMP, DMP, and NPP (Supporting Information Table S2), and these functions are then used to calculate the climate for the fossil floras using the V -scores of the fossil site. The standard error is here taken as the average residual prediction error of modern site scores.

2.2.2. Leaf Area Analysis

LAA employs the single-variate correlation between the average leaf area in a leaf assemblage and precipitation (Peppe et al., 2011; Wilf et al., 1998; Wright et al., 2017), to reconstruct MAP from fossil leaf assemblages. The correlation between leaf area and precipitation likely relies on optimizing area for photosynthetic leaf surface area while reducing water loss in response to atmospheric vapor pressure deficits (Parkhurst & Loucks, 1972; Wright et al., 2017). Here, we use two existing calibrations (Equation 3, Peppe et al., 2011, Equation 2, Wilf et al., 1998), as well as a novel calibration based on modern Australian mesothermal floras, including leaf assemblages of vegetation growing in $MAT > 17^\circ\text{C}$ and $MAP 40\text{--}400 \text{ cm yr}^{-1}$ (Equation 4; Supporting Information Table S3).

$$\ln(MAP) = 0.547 \times \ln A + 0.786 \quad (2)$$

$$\ln(MAP) = 0.283 \times \ln A + 2.92 \quad (3)$$

$$\ln(MAP) = 0.782 \times \ln A - 0.823 \quad (4)$$

In Equations 2–4, area (A) represents the averaged natural log of area of different leaf types for each fossil leaf assemblage (Supporting Information Table S4) and calculated MAP is in cm yr^{-1} .

2.2.3. Leaf Margin Analysis

LMA relies on the observed negative correlation between leaf margin teeth and MAT (Greenwood et al., 2004; Peppe et al., 2011; Wilf, 1997). It is likely no single mechanism explaining the occurrence of leaf teeth in woody dicots, but the negative correlation with temperature may be due to benefits in spring photosynthetic rates of deciduous taxa in cooler climates (Edwards et al., 2016; Royer & Wilf, 2006). In evergreen woody dicots, leaf teeth may aid in the guttation process, reducing root pressure through leaf hydathodes (Feild et al., 2005; Li et al., 2016; Reichgelt & Lee, 2021; Royer et al., 2009). Despite the absence of a uniform mechanism explaining the occurrence of leaf teeth, the negative correlation between leaf margin teeth and MAT can be observed globally (Peppe et al., 2011) and in Australia (Greenwood et al., 2004), suggesting that despite the role that water availability may play the LMA proxy has utility in Australia. In this study, we used two LMA calibrations to calculate MAT: a global calibration (Equation 5, Peppe et al., 2011) and a calibration based on modern-day Australian leaf assemblages (Equation 6, Greenwood et al., 2004).

$$MAT = 20.4 \times (1 - LMP) + 4.6 \quad (5)$$

$$MAT = 27 \times (1 - LMP) - 2.12 \quad (6)$$

In Equations 5 and 6, LMP (Leaf Margin Percentage) represents the fraction of leaves with toothed margins (Supporting Table S5), and calculated MAT is in $^{\circ}\text{C}$. Standard deviation of MAT is calculated using the method of Wilf (1997).

$$\sigma[MAT] = c \sqrt{\frac{LMP \times (1 - LMP)}{n}} \quad (7)$$

In Equation 7, c is the slope in Equations 5 and 6 and n is the number of morphotypes in the assemblage (Supporting Information Table S5).

2.3. Nearest Living Relatives

Plant fossil-based NLR techniques such as the coexistence analysis and bioclimatic analysis use the modern-day climatic ranges of plant taxa co-occurring in a fossil assemblage and generating an envelope of possible overlap (Greenwood et al., 2003; Kershaw, 1997; Utescher et al., 2014). In this study, we use the modern-day distributions of co-occurring plant taxa to generate the highest likelihood envelope of overlap, using a probability density approach (Greenwood et al., 2017; West et al., 2020, 2021; Willard et al., 2019). Using this probability density approach reduces subjectivity, for example, when taxa co-occur in a fossil assemblage that does not have a modern-day climatic range overlap, which is common in Southern Hemisphere paleofloras (e.g., Reichgelt et al., 2015).

Modern-day occurrence data of plant groups identified from each site (Supporting Information Table S6) was obtained from the Global Biodiversity Information Facility (GBIF [2021]); for links to occurrence datasets of specific plant taxa see Supporting Information Table S6). The occurrence datasets were subjected to a rigorous filter by eliminating exotic and cultivated occurrences, duplicate occurrences, and minimizing regional climatic biasing by randomly eliminating occurrences from oversampled areas until sample density was homogenous throughout a plant group's range. The means (μ) and standard deviations (σ) of the climatic range of each plant group (Supporting Information Table S6) were then calculated by extracting point-specific climatic data for the remaining geodetic coordinates using the *dismo* package in R (Hijmans et al., 2005).

A random set of 250,000 unique geodetic coordinates was then generated and climate data were extracted for these coordinates in the same manner as described above. The probability (f) for each plant group (t) occurring at each of these climates was then calculated using the product of probabilities of individual climate parameters (c).

$$f(t_n) = \prod_{i=1}^m \frac{1}{\sqrt{2\sigma_c^2} \times \pi} e^{x_c - \mu_c / 2\sigma_c^2} \quad (8)$$

In Equation 8, the number of climatic variables used to calculate the probability of this plant group (t) occurring at this combination of climatic variables is represented by m , whereas n represents the number of plant groups in the assemblage, x_c is a specific value of a climatic variable for which the probability is being tested, and μ_c and σ_c are the mean and standard deviation of the climatic range of the plant group that is being evaluated. Then, the probability of each climatic combination for all plant groups combined can be calculated with the product of the results produced by Equation 8.

$$f(z) = \prod_{i=1}^n f(t_n) \quad (9)$$

The combination of climatic variables with the highest $f(z)$ is the value that is presented in the results. The 95% confidence interval is the maximum range of climate variables with $f(z) \geq 5\%$ of the maximum $f(z)$. Five climatic variables were reconstructed using the NLR approach here (MAT, WQT, CQT, MAP, and DMP).

2.4. Ensemble Climate Approach

Individual plant-based paleoclimate proxies have biases due to a variety of reasons, such as evolutionary history, taphonomy, and shortcomings in calibration data (e.g., Greenwood, 2005, 2007; Grimm & Potts, 2016; Hagen et al., 2019; Kennedy et al., 2014; Little et al., 2010; Spicer et al., 2005, 2011). Nevertheless, since plants are sessile organisms, interacting directly with their environment, their physiognomy and distribution are a direct expression of their environment, making plant fossils robust indicators of terrestrial paleoclimate. LAA, LMA, and CLAMP all rely on leaf physiognomy, but on unique calibration datasets and are thus semi-independent proxies, whereas NLR is based on taxonomy, not physiognomy, and therefore fully independent from the other leaf physiognomy-based proxies. In this study, we produce ensemble paleoclimate estimates based on the results of the individual proxy estimates to generate paleoclimate estimates that take the uncertainty of each approach into account (Greenwood et al., 2017; Lowe et al., 2018; West et al., 2020). This approach is inclusive, generating an ensemble mean and standard deviation that accounts for uncertainty arising from each proxy, rather than choosing a single method that may suffer an undetected systematic bias. Additionally, this approach reveals when proxies produce anomalous results.

Ensemble estimates are generated by resampling ($n = 1000$) individual proxy estimates using the means and standard deviations of those results, assuming a bell-shaped probability distribution. The climatic variables for which we generate ensemble estimates are MAT, WQT, CQT, MAP, and DMP. MAT, CQT, and WQT estimate from LMA or CLAMP are resampled following a normal distribution. MAP and DMP from LAA and CLAMP are resampled following a log-normal distribution. All climatic variables generated from NLR are non-normally distributed and we, therefore, did not assume a bell-shaped probability distribution for resampling but instead resampled randomly within the 95% confidence interval. Because multiple calibrations were used for LAA and LMA, we first generated ensemble LAA and LMA estimates, before generating ensemble estimates that gave equal weight to each proxy.

2.5. Primary Productivity Reconstruction

Net primary productivity (NPP) is the rate at which photoautotrophs—principally plants—generate organic compounds from inorganic atmospheric carbon dioxide, minus the carbon that is subsequently lost to respiration. Without decomposition, terrestrial NPP represents the amount of carbon that is stored in plant biomass every year. Recently, Li et al. (2020) were able to demonstrate an empirical correlation between the average leaf area of vegetation and NPP. This correlation likely arises from large leaves being associated with warm humid climates, having a large surface area for gas exchange, and thereby maintaining high photosynthetic rates (e.g., Wright et al., 2017). Li et al. (2020) were able to reproduce NPP in North America using a calibration dataset from Asia, and vice versa, suggesting robustness in their approach. However, estimating primary productivity by remotely-sensed leaf area index measurements in the Southern Hemisphere has been problematic, due to

regional differences in leaf retention and physiognomy (e.g., Garrigues et al., 2008; Tian et al., 2004). Therefore, we obtained NPP values from MODIS (Running et al., 2015) for the Southern Hemisphere CLAMP calibration dataset (see Section 2.2.1) from 2012 to 2015 and generated a calibration for NPP (in $\text{gC m}^{-2} \text{yr}^{-1}$) for Southern Hemisphere fossil leaf assemblages. We found an average residual error of NPP estimates of $336 \text{ gC m}^{-2} \text{yr}^{-1}$ in this calibration dataset. However, residual error was distributed unequally, as large-leaved (predominantly mesophyll) assemblages in the Southern Hemisphere calibration dataset had consistently high NPP, but small-leaved (micro- and leptophyll) assemblages showed greater uncertainty (Supporting Information Table S2).

2.6. Biomes

The most similar modern biomes or vegetation types of our fossil floras were reconstructed with two independent methods in this study. First, ensemble estimates for MAT and MAP were plotted on Whittaker biome plots (Whittaker, 1962) and compared to modern-day biomes. Second, CLAMP-derived leaf physiognomy scores of fossil floras were compared to modern Southern Hemisphere floras using principal component analysis (PCA) and hierarchical cluster analysis (HCA). PCA was performed using the stats package in R (R Core Team, 2020). A Euclidean dissimilarity matrix was generated using the cluster package in R (Maechler et al., 2021), after which HCA was performed with Ward's minimum variance agglomeration method (Ward, 1963) using the stats package in R (R Core Team, 2020).

2.7. Comparison to Global Climate Models

Proxy reconstructions were compared to results from early Eocene global climate models (GCMs). The purpose of this comparison is partly to evaluate the model simulations at the locations of the proxy data, and partly to provide a broader regional and global perspective on the results presented in this study. We use simulations from the Deep-time Model Intercomparison Project (DeepMIP) (Lunt et al., 2017, 2021). DeepMIP simulations exist from eight models, covering a range of atmospheric CO_2 concentrations from 1 to $9\times$ the preindustrial value, with the paleogeography and vegetation from Herold et al. (2014), and preindustrial levels of non- CO_2 greenhouse gases and Earth orbital parameters. Here we employ the early Eocene climate simulations from the Community Earth System Model version 1.2 (CESM1.2) run with a resolution of $1.9^\circ \times 2.5^\circ$ (longitude \times latitude) and the GFDL Climate Model version 2.1 (GFDL_CM2.1) run with an atmosphere resolution of $3^\circ \times 3.75^\circ$, both at CO_2 concentrations of $6\times$ the preindustrial value. This is because these two simulations have been found to be the most consistent with a combination of global estimates of CO_2 , mean annual temperature, and meridional temperature gradient (see Figures 1a and 1b in Lunt et al. [2021]). CESM1.2 and GFDL_CM2.1 are global climate models that include model components of atmosphere, ocean, land surface, and sea ice. Details of the CESM1.2 simulations can be found in J. Zhu et al. (2019), and details of the GFDL_CM2.1 simulations can be found in Lunt et al. (2021) with additional information about the model itself in Hutchinson et al. (2018).

3. Results

3.1. Temperature

Following the climate scheme of Belda et al. (2014) most proxy reconstructions produce congruent subtropical temperature estimates for all sites (Table 2): MAT estimates are predominantly $17\text{--}23^\circ\text{C}$ and CQT are $12\text{--}18^\circ\text{C}$, compared to a MAT of $12\text{--}18^\circ\text{C}$ and average winter temperatures of $9\text{--}13^\circ\text{C}$ in the region today (Bureau of Meteorology, 2009). These values indicate that during the early to middle Eocene, not all monthly mean temperatures are $>18^\circ\text{C}$ in southern Australia, which excludes a tropical classification, but 8–12 months with monthly mean temperatures $>10^\circ\text{C}$ were present at each site (Table 2), implying a subtropical climate in the context of modern climate zones (Belda et al., 2014). Ensemble estimates for MAT indicate that Deans Marsh and Dinmore may have had temperate climates, as their reconstructed ensemble MAT is $14.8 \pm 5.4^\circ\text{C}$ and $16.7 \pm 4.8^\circ\text{C}$, respectively (Table 3). Lower MAT values at Deans Marsh and Dinmore are the result of low reconstructed MAT by the LMA proxy: $2.5\text{--}12.4^\circ\text{C}$ for Deans Marsh and $5.7\text{--}15.0^\circ\text{C}$ for Dinmore (Table 2). When the results of the LMA proxy are omitted from the ensemble estimates, MAT reconstruction of Deans Marsh and Dinmore is consistent with the other sites (Table 3). The lower MAT reconstructed from LMA for Deans Marsh and Dinmore may reflect a taphonomic bias as water's edge deposits may be enriched in toothed species, depressing site MAT estimates by $2\text{--}5^\circ\text{C}$ (Burnham et al., 2001; Greenwood, 2005).

Table 2
Results of CLAMP, LAA, LMA and NLR Analyses

Site	Method	MAT (°C)	MDR (°C)	WQT (°C)	CQT (°C)	MAP (cm)	WMP (cm)	DMP (cm)	NPP kgC m ⁻² yr ⁻¹
Poole Creek	CLAMP	17.5–22.3	18.3–21.5	24.4–28.7	9.7–15.4	21–50	4.5–9.3	0.1–0.8	0.9–1.6
	LAA	-	-	-	-	27–134	-	-	-
	LMA	15.6–22.6	-	-	-	-	-	-	-
	NLR	18.5–21.7	-	21.6–26.3	12.9–18.3	95–166	-	2.1–6.2	-
Nelly Creek	CLAMP	21.7–26.5	22.5–25.7	27.5–31.8	15.3–21.0	23–53	3.4–6.8	0.3–2.1	0.8–1.5
	LAA	-	-	-	-	28–145	-	-	-
	LMA	10.7–19.6	-	-	-	-	-	-	-
	NLR	16.9–21.4	-	20.5–26.3	11.1–18.2	85–178	-	2.1–8.7	-
Deans Marsh	CLAMP	20.2–25.0	21.0–24.2	28.8–33.1	11.3–17.1	10–23	2.2–4.6	0.1–0.3	1.0–1.7
	LAA	-	-	-	-	36–145	-	-	-
	LMA	2.5–12.4	-	-	-	-	-	-	-
	NLR	17.7–21.3	-	20.0–24.5	13.0–19.1	126–219	-	3.6–9.8	-
Nerriga	CLAMP	15.2–20.0	16.0–19.2	20.9–25.2	8.0–13.7	49–116	10.5–21.4	0.3–1.7	1.0–1.7
	LAA	-	-	-	-	93–386	-	-	-
	LMA	17.0–22.4	-	-	-	-	-	-	-
	NLR	20.1–22.5	-	23.0–25.3	15.4–19.6	117–200	-	2.6–5.9	-
Golden Grove	CLAMP	17.0–21.8	17.8–21.0	23.0–27.3	9.5–15.2	36–86	7.8–16.0	0.2–1.2	0.9–1.6
	LAA	-	-	-	-	97–248	-	-	-
	LMA	14.4–21.1	-	-	-	-	-	-	-
	NLR	20.9–23.4	-	23.5–26.7	16.7–20.8	120–204	-	2.1–5.6	-
Maslin Bay	CLAMP	20.5–25.3	21.3–24.5	26.3–30.6	13.2–18.9	47–112	9.8–19.9	0.4–2.6	1.1–1.8
	LAA	-	-	-	-	111–446	-	-	-
	LMA	15.4–19.6	-	-	-	-	-	-	-
	NLR	20.0–21.6	-	23.0–24.8	15.6–18.7	132–191	-	3.4–7.1	-
Anglesea	CLAMP	20.0–24.8	20.8–24.0	25.1–29.4	14.2–20.0	63–149	11.0–22.5	1.1–6.8	1.2–1.9
	LAA	-	-	-	-	67–520	-	-	-
	LMA	13.3–19.9	-	-	-	-	-	-	-
	NLR	19.7–21.8	-	22.5–25.2	15.2–18.7	138–209	-	3.8–8.5	-
Dinmore	CLAMP	17.3–22.0	18.0–21.3	22.6–26.9	10.0–15.8	48–113	9.9–20.2	0.3–1.7	0.9–1.6
	LAA	-	-	-	-	65–257	-	-	-
	LMA	5.7–15.0	-	-	-	-	-	-	-
	NLR	17.3–20.5	-	21.7–25.5	11.1–16.7	102–178	-	2.8–7.2	-
Brandy Creek	LMA	18.0–23.4	-	-	15.2–17.6	138–204	-	-	-
	NLR	19.1–20.7	-	21.8–24.0	-	-	-	4.2–8.3	-
Hotham	LMA	15.5–21.5	-	-	14.5–16.9	148–204	-	-	-
Heights	NLR	18.2–20.2	-	21.3–23.6	-	-	-	4.9–8.9	-
Regatta Point	NLR	19.2–20.7	-	22.6–24.5	15.0–17.4	145–186	-	5.8–8.3	-
Lefroy & Cowran	NLR	18.5–20.2	-	21.8–23.6	14.5–16.9	138–191	-	4.7–8.5	-

Note. CLAMP: Climate Leaf Analysis Multivariate Program, LAA: Leaf Area Analysis, LMA: Leaf Margin Analysis, NLR: Nearest Living Relatives, MAT: Mean Annual Temperature, MDR: Mean Diurnal Range, WQT: Warmest Quarter Mean Temperature, CQT: Coldest Quarter Mean Temperature, MAP: Mean Annual Precipitation, WMP: Wettest Month Precipitation, DMP: Driest Month Precipitation, NPP: Net Primary Productivity.

Table 3
Results of Ensemble Analysis of Individual Proxy Paleoclimate Results

Site	MAT inc. LMA (°C)	MAT omit LMA (°C)	WQT (°C)	CQT (°C)	MAP (cm)	DMP (cm)
Poole Creek	19.8 (17.6–22.0)	19.9 (18.1–21.6)	25.2 (23.1–27.4)	13.9 (11.3–16.6)	66 (33–132)	1.0(0.2–4.0)
Nelly Creek	19.2 (17.9–20.6)	19.3 (17.9–20.6)	26.5 (22.8–30.1)	16.3 (13.4–19.3)	71 (34–146)	2.0(0.7–5.8)
Deans Marsh	14.8 (9.3–20.2)	21.0 (18.7–23.4)	26.4 (21.7–31.0)	15.2 (12.5–17.8)	58 (18–182)	0.9(0.1–7.3)
Nerriga	19.7 (17.2–22.1)	19.4 (16.9–22.0)	23.5 (21.8–25.2)	14.0 (10.0–18.1)	125 (74–213)	1.6(0.5–4.8)
Golden Grove	19.9 (17.3–22.5)	20.9 (18.6–23.1)	25.2 (23.5–26.9)	15.7 (11.8–19.5)	110 (62–194)	1.3(0.4–4.2)
Maslin Bay	20.3 (17.7–23.0)	21.8 (19.8–23.7)	26.2 (23.4–29.0)	16.6 (14.4–18.9)	127 (70–231)	2.3(0.8–6.3)
Anglesea	19.8 (16.7–22.9)	21.5 (19.5–23.4)	25.5 (23.1–27.9)	16.9 (14.7–19.1)	135 (74–247)	4.1(1.9–8.8)
Dinmore	16.7 (11.8–21.5)	19.2 (17.5–21.0)	24.2 (22.3–26.1)	13.4 (11.0–15.8)	108 (67–176)	1.7(0.5–5.6)
Brandy Creek	20.3 (18.7–22.0)	-	-	-	-	-
Hotham Heights	18.9 (17.4–20.5)	-	-	-	-	-

Note. LMA: Leaf Margin Analysis, MAT: Mean Annual Temperature, WQT: Warmest Quarter Mean Temperature, CQT: Coldest Quarter Mean Temperature, MAP: Mean Annual Precipitation, DMP: Driest Month Precipitation. Range indicates $\pm 1\sigma$.

Ensemble estimates of WQT and CQT are consistent across sites, with WQTs of 24–26°C and CQTs of 14–16°C (Table 3). However, there is a disagreement between proxy reconstructions of CLAMP and NLR, as CLAMP reconstructs larger differences between WQT and CQT than NLR (Table 2). Specifically, at Nelly Creek, Deans Marsh and Maslin Bay reconstructed WQT can be >30°C within 1SD using CLAMP, whereas WQT = 26.7°C is the maximum using NLR (Table 2). There is more consistency between CLAMP and NLR for CQT reconstructions; however, reconstructions of Nerriga and Golden Grove do not overlap within error (Table 2). CQT estimates that are consistently above 10°C indicate that frost in these floras would have been exceedingly rare. Larger seasonal temperature differences and higher WQT, as suggested by CLAMP reconstructions, would imply more continental conditions in early to middle Eocene southern Australia, similar to Mediterranean climates (Belda et al., 2014). The seasonal temperatures suggested by NLR would imply more moderate conditions, as produced on land in close proximity to the ocean and with high summer cloud cover (Kottek et al., 2006). MDR was only reconstructed using CLAMP and as such it suggests similar continental conditions as WQT, with consistent high MDR (mean $\pm 1SE > 21^\circ\text{C}$) for Nelly Creek, Deans Marsh, Maslin Bay, and Anglesea (Table 2).

3.2. Precipitation

Individual proxy mean annual precipitation (MAP) reconstructions range from 18 cm yr⁻¹ at Deans Marsh to 247 cm yr⁻¹ at Maslin Bay (Table 3)—lower than present-day rainforest climates in the Whittaker biome classification (Figure 2a). Poole Creek, Nelly Creek and Deans Marsh all have mean ensemble MAP estimates of ~65 cm yr⁻¹, whereas for Nerriga, Golden Grove, Maslin Bay, Anglesea, and Dinmore mean ensemble MAP reconstructions are >100 cm yr⁻¹ (Table 3). The ensemble MAP $\pm 1SD$ range is large for each site (>100 cm, except Poole Creek). This large uncertainty arises from proxy disagreement, with CLAMP consistently producing the lowest MAP estimates at each site, LAA producing a large range of MAP estimates within 1SD and NLR estimates consistently higher than CLAMP, but overlapping with LAA (Table 2).

Ensemble driest month precipitation (DMP) estimates show a substantial dry season, with mean estimates ranging from 0.9 cm month⁻¹ at Deans Marsh and 4.1 cm month⁻¹ at Anglesea (Table 3). Golden Grove has the lowest percent of DMP compared to average monthly precipitation, 13% and the highest is at Anglesea with 34%. However, the range of DMP estimates, similar to the range of MAP estimates, is substantial, with DMP $\pm 1SD$ ranges of >6 cm month⁻¹, amounting to a 60× difference between the highest and the lowest DMP of the range (Table 3). The resulting discrepancy could mean that the DMP receives about 5%–65% of the average monthly precipitation. The large range of DMP ensemble estimates arises from a consistent discrepancy between reconstructed DMP by CLAMP and NLR (Table 2). CLAMP produces DMP estimates that are consistently lower than those of NLR, with the two proxies having overlapping error ranges only at Anglesea (Table 2). Because CLAMP MAP estimates are also consistently lower than NLR estimates, CLAMP does reconstruct similar precipitation

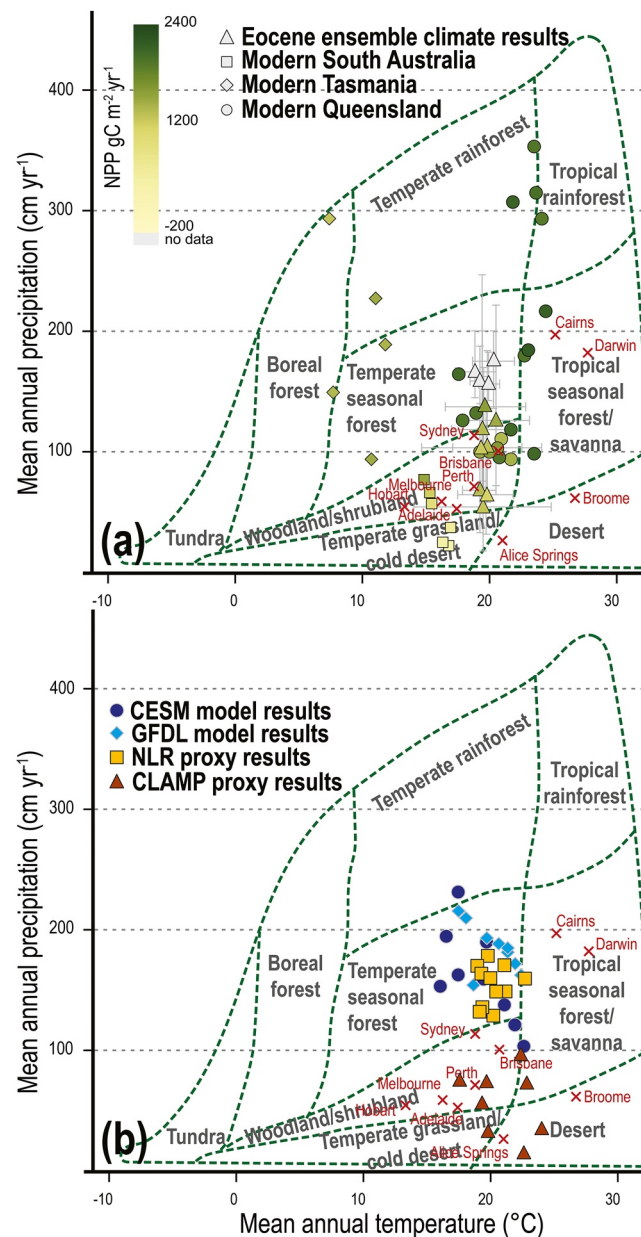


Figure 2. Whittaker vegetation plot (Whittaker, 1962) using mean annual precipitation (MAP) and mean annual temperature (MAT) of (a) modern calibration sites from South Australia (squares), Tasmania (diamonds) and Queensland (circles) (Supporting Information Table S2), and Eocene ensemble proxy reconstructions (triangles) excluding the results of leaf margin analysis (Table 3). Error bars indicate $\pm 1\sigma$ of reconstructed MAT and MAP (Table 3). Net Primary Productivity (NPP) is included for modern sites (Supporting Table S2) as well as Eocene sites for which NPP was reconstructed (Table 2). *Note.* the four Eocene sites with no NPP shading are Brandy Creek, Hotham Heights, Lefroy & Cowran, and Regatta Point, for which no NPP estimate was generated. Ensemble reconstructions place Eocene sites mainly in the Temperate Seasonal Forest biome, similar to modern Sydney and Brisbane, but with lower NPP. Inland and northern sites are in the Woodland/shrubland biome, similar to modern day Perth. (b) Comparison of site specific Eocene climate at 6x pre-industrial carbon dioxide levels obtained by point extractions using the Community Earth System Model version 1.2 (circles, CESM) and GFDL Climate Model version 2.1 (diamonds, GFDL), compared to the mode of Nearest Living Relative proxy reconstructions (squares, NLR) and the mean of Climate Leaf Analysis Multivariate Program proxy reconstructions (triangles, CLAMP) (Table 2). This shows the broad overlap in MAP and MAT of NLR proxy reconstructions, CESM and GFDL model output, and consistent placement of each site within the Temperate Seasonal Forest biome, with more precipitation than present-day Brisbane and Sydney, but cooler than Cairns and Darwin. CLAMP MAP estimates are distinctly anomalous, indicating biomes that span Woodlands to Desert, similar to present-day Perth and Alice Springs.

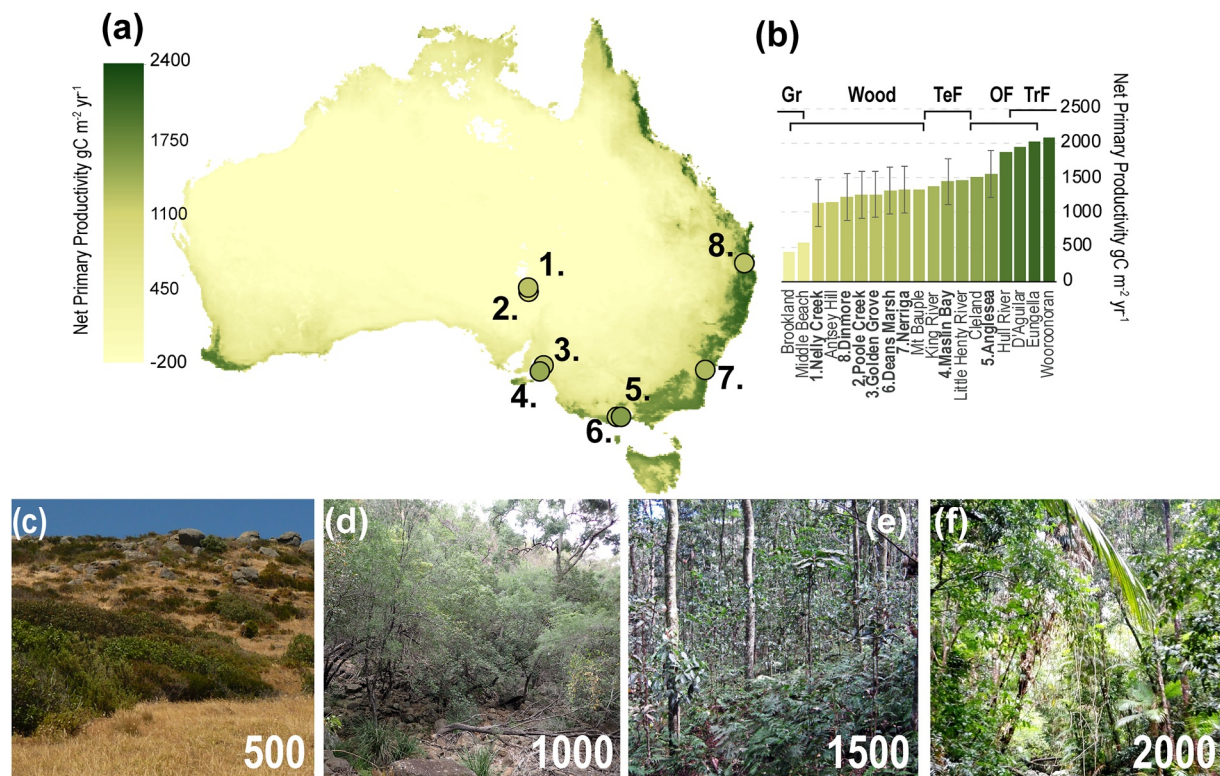


Figure 3. Map of modern-day Australia Net Primary Productivity (NPP) from MODIS (Running et al., 2015) with Eocene megafossil site reconstructed NPP for comparison (Table 2), 1. Nelly Creek, 2. Poole Creek, 3. Golden Grove, 4. Maslin Bay, 5. Anglesea, 6. Deans Marsh, 7. Nerriga, 8. Dinmore. (b) Histogram with Eocene and selected modern calibration site NPP (Supporting Information Table S2), with broad modern vegetation type indicated, Gr: grassland, Wood: woodland, TeF: temperate rainforest, OF: open forest, TrF: tropical rainforest. (c) Shrubland at Rosetta Head, South Australia, representative of relatively low NPP ecosystems that are typical of modern-day southern Australia. None of the Eocene sites have similar NPP to this ecosystem. Picture by TR. (d) Semi-evergreen vine thicket at Mount Kaputar, New South Wales, representative of moderately low productivity ecosystems that the Nelly Creek, Poole Creek and Dinmore sites are similar to. Picture by JGC. (e) Notophyll vine forest at Mount Cordeaux, south Queensland, representative of moderately high NPP ecosystems that the Anglesea and Maslin Bay sites are similar to. Picture by JGC. (f) Mesophyll vine forest at the Daintree Rainforest Observatory, northern Queensland, representative of the highest NPP ecosystems in Australia today. None of the Eocene sites have similar NPP to this ecosystem. Picture by TR.

seasonality as the ensemble estimates, with the DMP comprising 10% of the average monthly precipitation at Deans Marsh and 34% at Anglesea.

3.3. Primary Productivity

Reconstructed NPP for early to middle Eocene southern Australian sites is uniformly 1,100–1,600 $\text{gC m}^{-2} \text{yr}^{-1}$ by CLAMP (Table 2). In the inland and South Australian sites, reconstructed Eocene NPP is higher than NPP of the modern-day location of the site (Figure 3a). Modern-day locations with similar NPP in Australia range from *Eucalyptus* woodland to temperate rainforests, but are not in the range of subtropical to tropical rainforests with year-round growing seasons (Figure 3b). Nelly Creek, Poole Creek, and Dinmore have the lowest reconstructed NPP ($<1,300 \text{gC m}^{-2} \text{yr}^{-1}$), which are also the northernmost floras (Figure 3a).

3.4. Biomes/Vegetation Character

The combination of MAT and MAP places all early to middle Eocene Australian sites investigated here in the woodland-shrubland to temperate seasonal forest biomes of the Whittaker vegetation plot (Figure 2a). The sites do not have a high enough MAP to be considered temperate rainforest under this biome scheme, nor is the MAT high enough to be considered tropical. Dinmore and Deans Marsh have the lowest reconstructed MAT and therefore plot closely to modern South Australian woodland and shrubland sites. However, if the LMA analysis

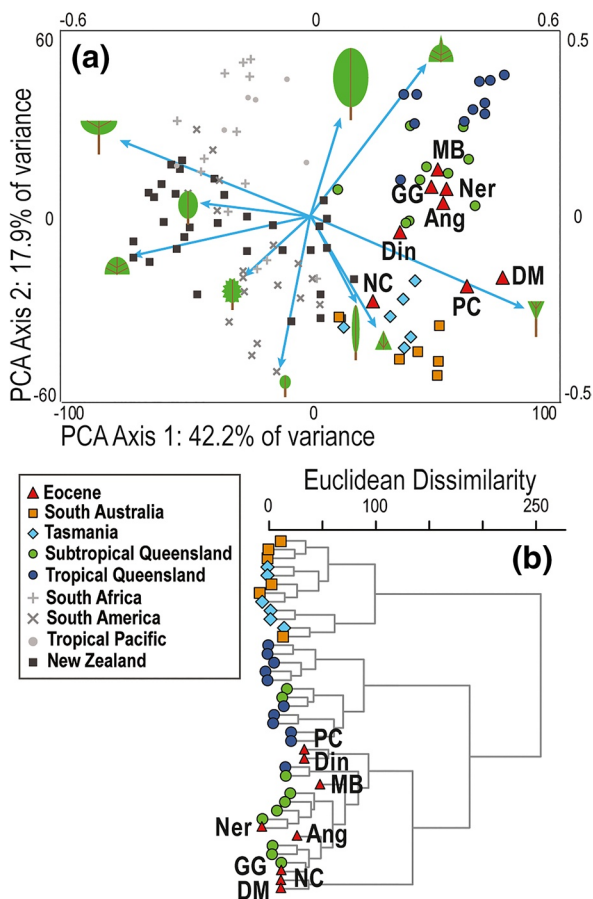


Figure 4. Results of Principal Components (a) and Hierarchical Cluster (b) Analyses. Eocene leaf physiognomy (diamonds) in comparison to modern Australian and other Southern Hemisphere leaf physiognomy calibration sites (Supporting Information Table S1). In panel (a) vectors scores are accompanied by schematic representations of different leaf characters (Supporting Information Table S1). PC: Poole Creek, NC: Nelly Creek, DM: Deans Marsh, GG: Golden Grove, Din: Dinmore, MB: Maslin Bay, Ner: Nerriga and Ang: Anglesea.

is omitted from the ensemble analysis (Table 3) then Dinmore is similar to modern-day drier subtropical Queensland sites and Deans Marsh would be similar to Nelly and Poole Creek (Figure 2a).

PCA on leaf physiognomy of Eocene Australian and modern-day Southern Hemisphere leaf assemblages reveals that modern and Eocene Australia share more physiognomic similarities than other Southern Hemisphere localities (Figure 4a). Specifically, Australian leaves have more attenuate leaf apices, acute leaf bases and apices, and higher length to width ratios. The PCA also reveals that analogous to the Whittaker vegetation plots (Figure 3a), the Maslin Bay, Nerriga, Golden Grove, Anglesea, and Dinmore floras are physiognomically similar to modern-day subtropical Queensland vine forests (Figure 4a). This similarity is seen in the HCA result that shows Maslin Bay, Nerriga, Anglesea, and Golden Grove physiognomies are more dissimilar to each other than to modern-day subtropical Queensland (Figure 4b). Conversely, PCA suggests physiognomic similarities between modern-day Tasmania and South Australia and the Nelly Creek, Deans Marsh, and Poole Creek floras (Figure 4a). However, HCA shows that these floras and Dinmore are more dissimilar to any of the modern floras, but that subtropical Queensland still has the most similar leaf physiognomy (Figure 4b). In addition to the results of the Whittaker vegetation plot, PCA and HCA show that Maslin Bay, Nerriga, Anglesea, and Golden Grove analogs may be found in modern-day subtropical Queensland, but that modern analogs for Poole Creek, Dinmore, Nelly Creek and Deans Marsh were either not included in our analysis, or do not exist in the modern world.

3.5. Comparison to Global Climate Models

Proxy results were compared to the GFDL and CESM simulations at $\times 6$ preindustrial CO_2 levels (Hutchinson et al., 2018; J. Zhu et al., 2019), since these simulations have provided good model-proxy comparisons for the early Eocene previously (Lunt et al., 2021; but see Supporting Information Table S7 for modeled results at different CO_2 levels). MAT proxy estimates were comparable to model results at the same locations as CLAMP and NLR (RMSE = 2.7°C and 2.5°C, respectively; Figures 5a and 5b). However, model simulations compared poorly to proxy results of LMA (RMSE = 6.0°C). For WQT (RMSE = 4.0°C) and CQT (RMSE = 3.1°C), CLAMP is generally better aligned with model results than NLR (RMSE = 5.6°C and 5.1°C)

(Figures 5c–5f). NLR produces WQT estimates that are lower than the models and CQT estimates that are higher than those of the models. This shows that the temperature seasonality of CLAMP corresponds better with modeled results than that of NLR, as NLR reconstructs a smaller seasonal temperature difference. Conversely, NLR reconstructions for MAP are well-aligned with modeled reconstructions (RMSE = 18.5 cm), whereas LAA (RMSE = 71.5 cm) and CLAMP (RMSE = 121.5 cm) are distinctly more poorly aligned with modeled results (Figures 5g and 5h). In particular, CLAMP produces systematically lower MAP estimates, whereas LAA results are more scattered. DMP proxy reconstructions are unaligned with modeled reconstructions (Figures 5i and 5j). CLAMP produces DMP estimates that are much lower than modeled results (RMSE = 8.5 cm), whereas NLR DMP estimates align somewhat better with modeled results, though still consistently lower (RMSE = 4.9 cm). Based on these results, it is evident that both model-proxy and proxy-proxy disagreements persist, specifically in seasonality reconstructions under hothouse climate conditions.

Despite discrepancies in precipitation and temperature seasonality reconstructions, model and NLR proxy results agree that the climate type in early to middle Eocene southern Australia would have supported temperate seasonal forest in the Whittaker (1962) biome scheme (Figure 2b). However, because of much lower MAP estimates, reconstructed vegetation type according to CLAMP differs from model and NLR results, as reconstructed biomes range from woodlands to savanna and in some cases desert (Figure 2b).

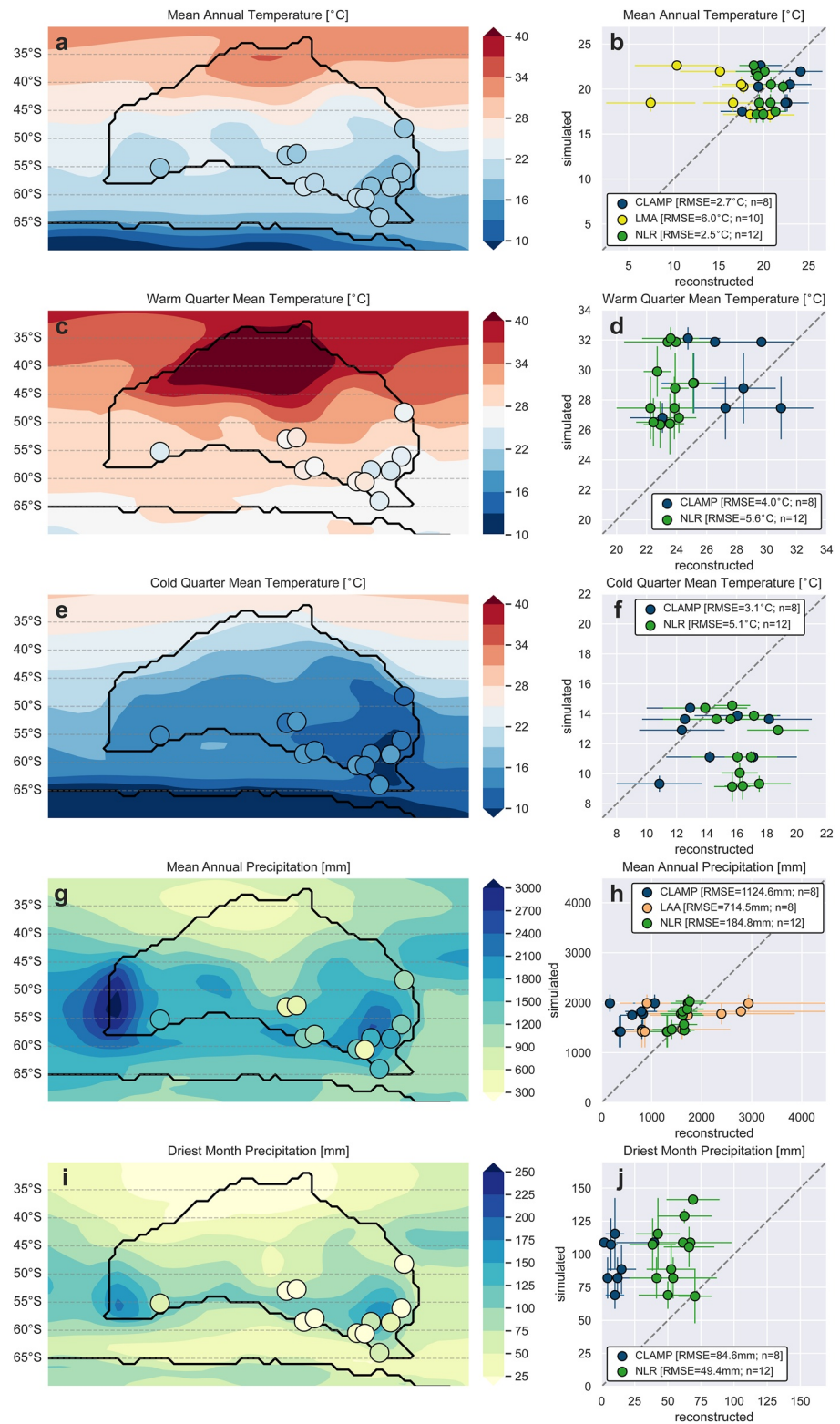


Figure 5. Comparison of Eocene point climate data extraction from the Community Earth System Model version 1.2, GFDL Climate Model version 2.1 and proxy reconstructions, Nearest Living Relatives (NLR), Leaf Margin Analysis (LMA), Climate Leaf Analysis Multivariate Program (CLAMP), Leaf Area Analysis (LAA). Maps show joint averages of models in comparison to ensemble reconstructions (Table 3), whereas graphs show averages of models in comparison to individual proxy reconstructions. (a),(b) Mean annual temperature, (c),(d) Warm quarter mean temperature, (e),(f) Cold quarter mean temperature, (g),(h) Mean annual precipitation, (i),(j) Driest month precipitation.

4. Discussion

4.1. Proxy Discrepancies

Ensemble analysis allows us to address and evaluate observed proxy discrepancies, which may inform proxy applicability for future studies. In this study, LMA produces anomalously lower MAT estimates than CLAMP and NLR, which is particularly clear at the Deans Marsh and Dinmore localities (Table 2; Figure 5b). LMA is based on a single-variate negative correlation between the percentage of toothed leaf types or species in an assemblage and MAT (e.g., Wilf, 1997). This negative correlation has been shown to exist in Australia, though the regression function deviates from other Northern Hemisphere regressions (Greenwood et al., 2004). The mechanism that underpins a selective advantage for toothed leaves in cooler climates is debated, with proposed mechanisms such as greater photosynthetic activity along serrated margins in early spring (Royer & Wilf, 2006) and dissected leaves being able to acquire more area within the bud before leaf burst (Edwards et al., 2016). Importantly, both these mechanisms are especially advantageous to deciduous plants, as both were investigated in winter-deciduous plants. Leaf teeth in evergreen angiosperms may be related to water availability, with positive correlations between leaf teeth and water availability identified in China, Australia, and New Zealand (Li et al., 2016; Reichgelt & Lee, 2021; Royer et al., 2009). The mechanism that provides a selective advantage to toothed leaves in wetter climates is the release of root water pressure at night through hydathodal teeth (Feild et al., 2005). Specific functions of leaf teeth are often not studied, but a study of leaf teeth in xeric shrubland and savannas in north-eastern Brazil found that hydathodal teeth were the most common (Moreira Rios et al., 2020). Taken together, as noted prior there is a risk that fossil flora taphonomy, such as proximity to a stream or a local high water table, leads to a MAT underestimation from LMA (Burnham et al., 2001; Greenwood, 2005). Greenwood (2005) noted a marked deviation from expected MAT using LMA for leaf litter assemblages collected from streams at MAT <16°C and recommended considering the LMA-water's edge effect in the analysis of Australian fossil leaf assemblages, especially where species richness was low. CLAMP suffers less from this potential taphonomic overprinting since it uses multivariate analysis to find the closest physiognomic analog based on the convergence of numerous leaf characteristics and climatic parameters (e.g., Spicer et al., 2005, 2011). CLAMP can therefore identify the highest convergence with modern analog floras with a relatively high number of toothed leaves that are mesothermic but riparian, rather than only associating this trait with microthermic climates. Conversely, LMA is a linear correlation method, with one input and output, which cannot account for the potential effect of other environmental variables than MAT on its proxy input. Given this pitfall and the clear discrepancy of the LMA results of Dinmore and Deans Marsh with the other proxy results, we interpret the results of the ensemble analysis with LMA omitted (Table 3).

While CLAMP and NLR produce generally harmonious MAT results in this study, WQT and CQT results are not (Table 2, Figures 5d and 5f). CLAMP suggests larger temperature seasonality and a generally more continental climate, whereas NLR suggests less seasonality. The mechanism behind this is unclear, but it highlights discrepancies between physiognomy- and taxonomy-derived proxies. CLAMP produces estimates based on similarities in leaf physiognomy, and NLR based on similarities in the taxonomic makeup of the assemblage. Interestingly, the CLAMP modern calibration sites maximum WQT is 26.9°C (Supporting Information Table S2), showing that CLAMP extrapolated WQT values of Nelly Creek, Deans Marsh, Maslin Bay, and Anglesea beyond the calibration data (Table 2). NLR cannot extrapolate beyond modern-day climates, but several taxa used in this study for NLR analysis do have distributions with mean WQT > 26.9°C (*Byblis*, *Rhizophora*, Nypoideae, *Lophostemon*, and Parkerioideae; Supplementary Information Table S6). However, these taxa do not make up a large enough number of taxa per site to result in NLR WQT estimates of >26.9°C. CLAMP and NLR also produce divergent precipitation estimates, with MAP reconstructed by CLAMP generally lower than by NLR (Table 2, Figure 5h). LAA MAP estimates in all cases are between and overlap with the CLAMP and NLR reconstructed values. Wilf et al. (1998) point out that since CLAMP scores leaf area categorically, rather than as a continuum, such as is done in LAA, larger leaves that are typically associated with rainy climates may be underrepresented. This may skew CLAMP precipitation resulting in drier reconstructed climates. Reconstructed DMP also diverges between CLAMP and NLR, with CLAMP reconstructions suggesting greater seasonality than NLR. In general, CLAMP reconstructions indicate a greater seasonality, both for temperature and precipitation, and a more continental climate in early to middle Eocene Australia than NLR.

Discrepancies between NLR and CLAMP could indicate that the studied fossil floral assemblages lack modern climatic analogs, taxonomically or physiognomically. The closer correspondence of proxy-reconstructed

temperature seasonality by CLAMP than NLR with model estimates (Figures 5c–5f) may indicate that the genera that comprised southern Australian floral assemblages during the early-middle Eocene have since adapted to different seasonality niches. In contrast, the closer correspondence of NLR than CLAMP precipitation estimates with model estimates (Figures 5g–5j) may indicate that the leaf physiognomy of mesothermic Australian forests growing at 50–65°S has no modern analog growing in similar precipitation regimes, likely reflecting the high latitude light seasonality of the Eocene which may have favored deciduousness (e.g., Greenwood & Christophel, 2005; Greenwood et al., 2003; West et al., 2020). However, the disparity in precipitation and seasonality proxy reconstructions is mirrored in climate models, which may simply indicate that in the terrestrial realm, the response of precipitation and seasonality to elevated temperatures is not well-understood.

4.2. Early to Middle Eocene Southern Hemisphere Paleoclimate

Ensemble reconstructions from early to middle Eocene Australia consistently suggest a mesothermal (subtropical) terrestrial paleoclimate (MAT: 19–21°C) with precipitation of >100 cm yr⁻¹ near the coast and ~60 cm yr⁻¹ in inland areas (Tables 2 and 3). The proxy reconstructions presented in this study do not indicate a temperature decline from the Ypresian to the Lutetian and the Bartonian stages (Table 2), as might be expected from global temperature reconstructions from marine proxies (e.g., Cramwinckel et al., 2018; Evans et al., 2018; Westerhold et al., 2020), or regional marine temperatures (Bijl et al., 2013; Douglas et al., 2014; Inglis et al., 2015). A potential decoupling in the magnitude of marine and terrestrial temperature changes in the early to middle Eocene in southern Australia has also been found using molecular proxies (Bijl et al., 2013) and from prior paleobotanical studies, and is likely reflecting the northward displacement of the Australian continent away from Antarctica over this time interval (Greenwood & Christophel, 2005; Greenwood et al., 2003).

The best agreement with proxy and GCM MAT was achieved with GCM models run at 6× pre-industrial CO₂ (1,680 ppm; Supporting Information Table S7). Independent CO₂ proxy reconstructions for the early to middle Eocene range from ~200 ppm from paleosols (Hyland & Sheldon, 2013) to ~3,500 ppm from Boron isotopes (Pearson & Palmer, 2000), and different proxies produce strongly divergent results (e.g., Bijl et al., 2010; Cui & Schubert, 2018; Steinthorsdottir et al., 2019). Eocene GCM models used in this study (Lunt et al., 2021), suggest that a MAT of 19–21°C at 50–65°S could be maintained by CO₂ levels of ~1,680 ppm, which corresponds best to proxy reconstructions obtained with phytoplankton δ¹³C (Pagani et al., 2005, 2011; Witkowski et al., 2018) and certain plant stomata-based reconstructions (Grein et al., 2011; Retallack, 2009), consistent with best-fit atmospheric CO₂ during the Early Eocene Climatic Optimum (50 Ma) of 1,150–2,500 ppm (Hollis et al., 2019).

Eocene terrestrial paleoclimate reconstructions have been generated from similar latitudes in South America and New Zealand, which allow us to assess potential climate homogeneity across southern high latitudes in the early to middle Eocene. The Laguna del Hunco and Ligorio Márquez fossil floras, from Argentina and Chile, respectively, were deposited at 50–55°S (Carmichael et al., 2016) in the early Eocene and the Rio Turbio fossil flora was deposited at ~58°S in the middle Eocene (Hinojosa, 2005; Hinojosa, Armetso, et al., 2006; Hinojosa, Pesce, et al., 2006; Hinojosa & Villagrán, 2005; Wilf et al., 2005). Reconstructed MATs from Ligorio Márquez and Laguna del Hunco range from ~17 to 19.5°C, with MAPs of ~150–200 cm yr⁻¹ (Hinojosa, Pesce, et al., 2006). Reconstructed MAT for the Rio Turbio fossil flora was ~18°C, with a MAP of 150–200 cm yr⁻¹ (Hinojosa & Villagrán, 2005). These ranges overlap with our estimates from similar latitudes in southern Australia, albeit with the South American estimates tending toward cooler and wetter climates. The Otaio and Waipara River sections in New Zealand were deposited at ~55°S (Carmichael et al., 2016) and early to middle Eocene MAT there was 15–25°C and MAP 110–140 cm yr⁻¹ using a combination of geochemical and paleobotanical proxies (Pancost et al., 2013). The paleoclimatic record from New Zealand also suggests relative climatic stability throughout the Ypresian and Lutetian, similar to what we observe in southern Australia at that time.

4.3. The Southern Green Continent

The occurrence of broad-leaved fossil floras and palynofloral assemblages resembling those of modern mesic- or rainforests in the Eocene of southern Australia has long been interpreted as evidence for a more homogeneously forested landscape at that time (e.g., Christophel, 1994; Christophel & Greenwood, 1989; Greenwood, 1996; Greenwood & Christophel, 2005; Macphail et al., 1994; Truswell, 1993). By contrast, the modern-day Australian landscapes have ~3% rainforest and the majority of the continent's vegetation consists of grasslands, spinifex,

shrubland, and open sclerophyll forest and woodland, with most of the continent arid to semi-arid (Morton et al., 2011; Sullivan et al., 2012). As a result, across most of the country NPP is $\sim 0 \text{ gC m}^{-2} \text{ yr}^{-1}$, with the exception of the more densely forested areas that receive more rainfall (Figures 3a and Running et al., 2015). Our results show that during the early to middle Eocene, inland floras such as Poole and Nelly Creek, as well as areas that are now dominated by woodlands and sclerophyll forests, such as Golden Grove and Maslin Bay in South Australia, would have had NPPs of 1,100–1,400 $\text{gC m}^{-2} \text{ yr}^{-1}$ (Figure 3). This NPP is lower than the $>1,800 \text{ gC m}^{-2} \text{ yr}^{-1}$ of modern-day broad-leaved (sub-) tropical rainforests in Australia (Figure 3), which may be expected under more seasonal and lower light conditions at 48–64°S. Importantly, the Nelly and Poole Creek flora reconstructed NPP imply that NPP may have been $>1,000 \text{ gC m}^{-2} \text{ yr}^{-1}$ higher than the modern day continental interior. This suggests that the southern Australian continental interior was far more productive than today. However, it must be noted that the late Paleocene to middle Eocene Eyre Formation, in which the Poole and Nelly Creek floras were deposited, is associated with a large inland lake (Alley, 1998) which may have made the depositional environment less continental than it would be today.

The latitudinal position of the paleofloras investigated here was 48–64°S (Table 1), which places them southward of mid-latitude high-pressure systems, and within the southern westerly wind belt. Indeed, the highest modeled precipitation is in Eocene Western Australia (Figure 5g), which would have received the most direct supply of moisture from the incoming westerly winds. The higher than modern NPP and associated “greening” is likely in part due to Eocene southern Australia’s position within a zone of low pressure systems and westerly winds, supplying ample moisture. No paleofloras were recovered from northern Australia at paleolatitudes of 35–40°S, and we, therefore, have no NPP estimate from this region, but the modeled results suggest MAP of 300–900 mm yr^{-1} (Figure 5g), showing a clear decrease in moisture supply closer to subtropical latitudes. Eocene northern Australia MAP is higher than the lowest MAP of 100–300 mm yr^{-1} in the continental interior of Australia today (Bureau of Meteorology, 2009). Therefore, northern Australia during the early to middle Eocene would have likely still had higher than modern NPP than the modern Australian continental interior. However, these modern low MAP values are found at 25–30°S, which makes the Eocene latitudinal position an imperfect analog to modern Australian climate systems. Conversely, looking southward, there are very few landmasses between 48 and 64°S today. The Antarctic Peninsula reaches $\sim 63^\circ\text{S}$, or to $\sim 61^\circ\text{S}$ if the South Shetland Islands are included. These areas are almost entirely devoid of vegetation. Further north, on the west coast of southern South America (48–56°S), NPP can be up to 1,200 $\text{gC m}^{-2} \text{ yr}^{-1}$, though mostly $\sim 600 \text{ gC m}^{-2} \text{ yr}^{-1}$ (Running et al., 2015). By contrast, reconstructed NPP for early to middle Eocene southern Australia is 800–1,900 $\text{gC m}^{-2} \text{ yr}^{-1}$ (Table 2). This indicates that the NPP of early to middle Eocene Australia was both higher than modern southern Australia, but also as vegetation growing at the same latitude that southern Australian Eocene vegetation would have been growing at.

Leaf physiognomy suggests that the closest modern analogs to the early to middle Eocene forests of southern Australia can still be found in Australia as well (Figure 4a), possibly due to Australia’s geographic isolation since the Eocene, where limited floristic exchange happened between different Gondwanan components (Weston & Jordan, 2017). The physiognomic affinity of all the investigated Eocene megaflores here to subtropical Queensland forests suggests the widespread presence of forests in southern Australia, such as notophyll vine forest (*sensu* Webb, 1968, Figure 3e), during the Eocene. However, while Maslin Bay, Nerriga, Anglesea, and Golden Grove nest within modern subtropical Queensland forest physiognomy (Figure 4b), Nelly Creek, Poole Creek, Dinmore, and Deans Marsh are more dissimilar. The vegetation that produced the latter megaflores may be more open vegetation, as is also suggested by the Whittaker biome reconstruction (Figure 3a), such as semi-deciduous vine thickets (Webb, 1968, Figure 3d). This interpretation is in line with the interpretation of Nelly and Poole Creek megaflores being produced by potential interfluvial sclerophyllous plant communities (Greenwood et al., 2000).

In addition to a supercharged hydrological cycle (e.g., Carmichael et al., 2016; Kiehl et al., 2021; Shields et al., 2021) and the geographical position of southern Australia within the westerly wind belt (Figure 1) transporting moisture into the interior of the Australian continent (Figure 5), higher than modern atmospheric CO_2 may also have contributed to the enhanced NPP, and hence the “greening” of early to middle Eocene southern Australia, observed in this study. Increased availability of CO_2 effectively reduces the drought threshold for plants, as plants reduce their stomatal conductance and thus transpire less water in response to increased CO_2 (e.g., Cernusak, 2020; Cernusak et al., 2019). Such an increase in water-use efficiency under higher than modern CO_2 has also been observed in organically preserved early Miocene leaf fossils (Reichgelt et al., 2020) and would result in biosphere expansion into areas that would otherwise be too dry (Herold et al., 2011; Zhou et al., 2017).

Finally, higher than modern NPP may be attributable to a direct carbon fertilization effect, which is higher carbon assimilation due to increased photosynthesis as a result of the higher availability of atmospheric CO₂ (e.g., Zhu et al., 2016).

5. Conclusions

Paleobotanical proxy analyses of early to middle Eocene southern Australia, then situated at 48–64°S, reconstruct the presence of a subtropical climate, with MATs of 19–21°C. These MAT reconstructions are consistent across different proxies, except LMA which may have a taphonomic over-print, and align well with GCMs of the early Eocene. Ensemble MAP reconstructions are also overall consistent with GCMs, producing homogeneous near-coast MAP reconstructions of >100 cm yr⁻¹ and drier conditions further inland with ~60 cm yr⁻¹. These reconstructions would support continuous temperate seasonal forest across early to middle Eocene southern Australia. However, CLAMP reconstructions are inconsistent with MAP from model simulations and the other proxies, producing lower MAP that would support sparser vegetation such as woodland and scrubland. CLAMP-reconstructed and model-simulated temperature seasonality also suggest seasonal continental conditions, whereas NLR reconstructs less seasonality and more ocean moderated conditions.

The combination of higher temperatures and more homogeneous rainfall than modern allowed for southern Australia to sustain a continuous woody vegetation cover. Near-coast vegetation in Eocene southern Australia would likely have been most similar to forests found in modern-day subtropical Queensland, such as notophyll vine forests. Landlocked and vegetation further north in Australia differs from these forests, representing potentially more open woodlands and semi-deciduous vine thickets, although a direct physiognomic analog could not be identified here. Regardless, all analyzed Eocene paleofloras reconstructed annual NPP of 1,100–1,400 gC m⁻² yr⁻¹, including landlocked sites. This NPP is lower than the relatively limited amount of area with rainforest in Australia today, but vastly exceeds the desert scrub, grassland, and shrubland NPP that predominates the Australian mainland today. Our results suggest that southern Australia, when at paleolatitude of 48–64°S, represented a green and productive southern landmass, and that annual carbon exchange with the biosphere during the hothouse climate of the early to middle Eocene vastly exceeded the productivity potential of today.

Acknowledgments

Many thanks to paleobotanical community in Australia, Robert S. Hill, Raymond J. Carpenter, Mike S. Pole, and in particular the late David C. Christophel, for their decades-long efforts to establish fossil plant collections across southern Australia. Gregory J. Jordan and James R. P. Worth are acknowledged for establishing modern calibration leaf assemblages in Tasmania. This work was supported by the Natural Sciences and Engineering Research Council of Canada (NSERC) through Discovery Grants (DG 311934 and 2016-04,337) to DRG, and prior funding from the Australian Research Council to DRG (Grant Nos. A39802019 & SGS28/99) and JGC (DPI130104314). DKH acknowledges support from Swedish Research Council Grant 2016-03,912 and Australian Research Council grant DE220100279. The GFDL simulations were performed using resources from the Swedish National Infrastructure for Computing (SNIC) at the National Supercomputer Centre (NSC), partially funded by the Swedish Research Council Grant 2018-05,973. JGC also the School of Biological Sciences at the University of Adelaide for the provision of resources to undertake the research. DJL and SS thank NERC grant NE/P01903X/1: SWEET: Super-Warm Early Eocene Temperatures and climate: understanding the response of the Earth to high CO₂ through integrated modeling and data.

Data Availability Statement

Supporting tables S1 – 7 are made available through DRYAD (Reichgelt et al., 2022). Data in Supporting Tables S1–6 represents compiled data (Christophel & Blackburn, 1978; Hill, 1982; Christophel & Greenwood, 1987; Christophel et al., 1987; Greenwood, 1987, 1996; Clarke, 1994; Carpenter & Pole, 1995; Scriven et al., 1995; Pole & Macphail, 1996; Conran & Christophel, 1998; Barnes & Hill, 1999; Vadala & Greenwood, 2001; Conran et al., 2003, 2009; Greenwood et al., 2003, 2017; Carpenter et al., 2006; Basinger et al., 2007; Pole, 2007, 2019; Rozefelds et al., 2016, 2021). The DeepMIP Eocene simulations are available by following the instructions at <https://www.deepmip.org/data-eocene/> (Hollis et al., 2019).

References

- Alley, N. F. (1998). Cainozoic stratigraphy, palaeoenvironments and geological evolution of the Lake Eyre Basin. *Palaeogeography, Palaeoclimatology, Palaeoecology*, 144(3–4), 239–263. [https://doi.org/10.1016/S0031-0182\(98\)00120-5](https://doi.org/10.1016/S0031-0182(98)00120-5)
- Alley, N. F., Krieg, G. W., & Callen, R. A. (1996). Early tertiary Eyre Formation, lower Nelly Creek, southern Lake Eyre basin, Australia: Palynological dating of macrofloras and silcrete, and paleoclimatic interpretations. *Australian Journal of Earth Sciences*, 43(1), 71–84. <https://doi.org/10.1080/08120099608728236>
- Barnes, R. W., & Hill, R. S. (1999). *Ceratopetalum* fruits from Australian Cainozoic sediments and their significance for petal evolution in the genus. *Australian Systematic Botany*, 12(5), 635–645. <https://doi.org/10.1071/SB98014>
- Bar-On, Y. M., Philips, R., & Milo, R. (2018). The biomass distribution on Earth. *Proceedings of the National Academy of Sciences*, 115(25), 6506–6511. <https://doi.org/10.1073/pnas.1711842115>
- Basinger, J. F., Greenwood, D. R., Wilson, P. G., & Christophel, D. C. (2007). Fossil flowers and fruits of capsular Myrtaceae from the Eocene of south Australia. *Canadian Journal of Botany*, 85(2), 204–215. <https://doi.org/10.1139/B07-001>
- Beerling, D. J., & Royer, D. L. (2011). Convergent Cenozoic CO₂ history. *Nature Geoscience*, 4, 418–420. <https://doi.org/10.1038/ngeo1186>
- Beer, C., Reichjstein, M., Tomelleri, E., Ciais, P., Jung, M., Carvalhais, N., et al. (2010). Terrestrial gross carbon dioxide uptake: Global distribution and covariation with climate. *Science*, 329(5993), 834–838. <https://doi.org/10.1126/science.1184984>
- Belda, M., Holtanova, E., Halenka, T., & Kalvova, J. (2014). Climate classification revisited: From Köppen to Trewartha. *Climate Research*, 59, 1–13. <https://doi.org/10.3354/cr01204>

- Benbow, M. C., Alley, N. F., Callen, R. A., & Greenwood, D. R. (1995). Geological history and palaeoclimate. In J. H. Drexel, & W. V. Preiss (Eds.), *The geology of South Australia* (pp. 208–217). South Australian Geological Survey.
- Bijl, P. K., Bendle, J. A. P., Bohaty, S. M., Pross, J., Schouten, S., Tauxe, L., et al. (2013). Eocene cooling linked to early flow across the Tasmanian Gateway. *Proceedings of the National Academy of Sciences*, *110*(24), 9645–9650. <https://doi.org/10.1073/pnas.1220872110>
- Bijl, P. K., Houben, A. J. P., Schouten, S., Bohaty, S. M., Sluijs, A. R., Reichart, G., et al. (2010). Transient middle Eocene atmospheric CO₂ and temperature variations. *Science*, *330*(6005), 819–821. <https://doi.org/10.1126/science.1193654>
- Bijl, P. K., Schouten, S., Sluijs, A., Reichart, G.-J., Zachos, J. C., & Brinkhuis, H. (2009). Early Palaeogene temperature evolution of the southwest Pacific Ocean. *Nature*, *461*, 776–779. <https://doi.org/10.1038/nature08399>
- Bureau of Meteorology. (2009). *Average annual & monthly maximum, minimum, & mean temperature*. Retrieved from http://www.bom.gov.au/jsp/ncc/climate_averages/temperature/index.jsp
- Burnham, R. J., Pitman, N. C. A., Johnson, K. R., & Wilf, P. (2001). Habitat-related error in estimating temperatures from leaf margins in a humid tropical forest. *American Journal of Botany*, *88*(6), 1096–1102. <https://doi.org/10.2307/2657093>
- Carmichael, M. J., Lunt, D. J., Huber, M., Heinemann, M., Kiehl, J., LeGrande, A., et al. (2016). A model–model and data–model comparison for the early Eocene hydrological cycle. *Climate of the Past*, *12*, 455–481. <https://doi.org/10.5194/cp-12-455-2016>
- Carpenter, R. J., Hill, R. S., Greenwood, D. R., Partridge, A. D., & Banks, M. A. (2004). No snow in the mountains: Early Eocene plant fossils from Hotham Heights, Victoria, Australia. *Australian Journal of Botany*, *52*(6), 685–718. <https://doi.org/10.1071/BT04032>
- Carpenter, R. J., Hill, R. S., & Scriven, L. J. (2006). Palmately lobed Proteaceae leaf fossils from the middle Eocene of South Australia. *International Journal of Plant Sciences*, *167*(5), 1049–1060. <https://doi.org/10.1086/505537>
- Carpenter, R. J., Jordan, G. J., Macphail, M. K., & Hill, R. S. (2012). Near-tropical early Eocene terrestrial temperatures at the Australo-Antarctic margin, Western Tasmania. *Geology*, *40*(3), 267–270. <https://doi.org/10.1130/G32584.1>
- Carpenter, R. J., & Pole, M. (1995). Eocene plant fossils from the Lefroy and Cowan paleodrainages, Western Australia. *Australian Systematic Botany*, *8*(6), 1107–1154. <https://doi.org/10.1071/SB951107>
- Cernusak, L. A. (2020). Gas exchange and water-use efficiency in plant canopies. *Plant Biology*, *22*(51), 52–67. <https://doi.org/10.1111/plb.12939>
- Cernusak, L. A., Haverd, V., Brendel, O., Le Thiec, D., Guehl, J.-M., & Cuntz, M. (2019). Robust response of terrestrial plants to rising CO₂. *Trends in Plant Science*, *24*(7), 578–586. <https://doi.org/10.1016/j.tplants.2019.04.003>
- Chen, I.-C., Hill, J. K., Ohlemüller, R., Roy, D. B., & Thomas, C. D. (2011). Rapid range shifts of species associated with high levels of climate warming. *Science*, *333*(6045), 1024–1026. <https://doi.org/10.1126/science.1206432>
- Christophel, D. C. (1994). The early Tertiary macrofloras of continental Australia. In R. S. Hill (Ed.), *History of the Australian vegetation: Cretaceous to recent* (pp. 262–275). Cambridge University Press
- Christophel, D. C., & Blackburn, D. T. (1978). Tertiary megafossil flora of Maslin Bay, south Australia: A preliminary report. *Alcheringa: An Australasian Journal of Palaeontology*, *2*(4), 311–319. <https://doi.org/10.1080/03115517808527787>
- Christophel, D. C., & Greenwood, D. R. (1987). A megafossil flora from the Eocene of Golden Grove, south Australia. *Transactions of the Royal Society of South Australia*, *111*(3), 155–162.
- Christophel, D. C., & Greenwood, D. R. (1989). Changes in climate and vegetation in Australia during the Tertiary. *Review of Palaeobotany and Palynology*, *58*(2–4), 95–109. [https://doi.org/10.1016/0034-6667\(89\)90079-1](https://doi.org/10.1016/0034-6667(89)90079-1)
- Christophel, D. C., Harris, W. K., & Syber, A. K. (1987). The Eocene flora of the Anglesea locality, Victoria. *Alcheringa: An Australasian Journal of Palaeontology*, *11*(4), 303–323. <https://doi.org/10.1080/03115517808619139>
- Christophel, D. C., Scriven, L. J., & Greenwood, D. R. (1992). An Eocene megafossil flora from Nelly Creek, south Australia. *Transactions of the Royal Society of South Australia*, *116*(2), 65–76.
- Clarke, J. D. A. (1994). Evolution of the Lefroy and Cowan paleodrainage channels, Western Australia. *Australian Journal of Earth Sciences*, *41*(1), 55–68. <https://doi.org/10.1080/08120099408728113>
- Conran, J. G., Carpenter, R. J., & Jordan, G. J. (2009). Early Eocene *Ripogonum* (Liliales: Ripogonaceae) leaf macrofossils from southern Australia. *Australian Systematic Botany*, *22*(3), 219–228. <https://doi.org/10.1071/SB08050>
- Conran, J. G., & Christophel, D. C. (1998). A new species of triplinerved *Laurophyllum* from the Eocene of Nerriga, New South Wales. *Alcheringa: An Australasian Journal of Palaeontology*, *22*(4), 343–348. <https://doi.org/10.1080/03115519808619332>
- Conran, J. G., & Christophel, D. C. (2004). A fossil Byblidaceae seed from Eocene south Australia. *International Journal of Plant Sciences*, *165*(4), 691–694. <https://doi.org/10.1086/386555>
- Conran, J. G., Christophel, D. C., & Cunningham, L. (2003). An Eocene monocotyledon from Nelly Creek, central Australia, with affinities to Hemerocallidaceae (Liliana: Asparagales). *Alcheringa: An Australasian Journal of Palaeontology*, *27*(2), 107–115. <https://doi.org/10.1080/03115510308619551>
- Contreras, L., Pross, J., Bijl, P. K., Koutsoudendris, A., Raine, J. I., van de Schootbrugge, B., & Brinkhuis, H. (2013). Early to middle Eocene vegetation dynamics at the Wilkes land margin (Antarctica). *Review of Palaeobotany and Palynology*, *197*, 119–142. <https://doi.org/10.1016/j.revpalbo.2013.05.009>
- Cramwinckel, M. J., Huber, M., Kocken, I. J., Agnini, C., Bijl, P. K., Bohaty, S. M., et al. (2018). Synchronous tropical and polar temperature evolution in the Eocene. *Nature*, *559*, 382–386. <https://doi.org/10.1038/s41586-018-0272-2>
- Cui, Y., & Schubert, B. A. (2018). Towards determination of the source and magnitude of atmospheric pCO₂ change across the early Paleogene hyperthermals. *Global and Planetary Change*, *170*, 120–125. <https://doi.org/10.1016/j.gloplacha.2018.08.011>
- Douglas, P. M. J., Affek, H. P., Ivany, L. C., Houben, A. J. P., Sijp, W. P., & Sluijs, A. (2014). Pronounced zonal heterogeneity in Eocene southern high-latitude sea surface temperatures. *Proceedings of the National Academy of Sciences*, *111*(18), 6582–6587. <https://doi.org/10.1073/pnas.1321441111>
- Eberle, J. J., & Greenwood, D. R. (2012). Life at the top of the greenhouse Eocene world—A review of the Eocene flora and vertebrate fauna from Canada's High Arctic. *The Geological Society of America Bulletin*, *124*(1–2), 3–23. <https://doi.org/10.1130/B30571.1>
- Edwards, E. J., Spriggs, E. L., Chatelet, D. S., & Donoghue, M. J. (2016). Unpacking a century-old mystery: Winter buds and the latitudinal gradient in leaf form. *American Journal of Botany*, *103*(6), 975–978. <https://doi.org/10.3732/ajb.1600129>
- Evans, D., Sagoo, N., Renema, W., Cotton, L. J., Müller, W., Todd, J. A., et al. (2018). Eocene greenhouse climate revealed by coupled clumped isotope-Mg/Ca thermometry. *Proceedings of the National Academy of Sciences*, *115*(6), 1174–1179. <https://doi.org/10.1073/pnas.1714744115>
- Feild, T. S., Sage, T. L., Czerniak, C., & Iles, W. J. D. (2005). Hydathodal leaf teeth of *Chloranthus japonicus* (Chloranthaceae) prevent guttation-induced flooding of the mesophyll. *Plant, Cell and Environment*, *28*(9), 1179–1190. <https://doi.org/10.1111/j.1365-3040.2005.01354.x>
- Fick, S. E., & Hijmans, R. J. (2017). WorldClim 2: New 1-km spatial resolution climate surfaces for global land areas. *International Journal of Climatol*, *37*(12), 4302–4315. <https://doi.org/10.1002/joc.5086>
- Foster, G. L., Royer, D. L., & Lunt, D. J. (2017). Future climate forcing potentially without precedent in the last 420 million years. *Nature Communications*, *8*, 14845. <https://doi.org/10.1038/ncomms14845>

- Garrigues, S., Lacaze, R., Baret, F., Morisette, J. T., Weiss, M., Nickeson, J. E., et al. (2008). Validation and intercomparison of global Leaf Area Index products derived from remote sensing data. *Journal of Geophysical Research*, *113*(G2), D01103. <https://doi.org/10.1029/2007JG000635>
- Gayó, E., Hinojosa, L. F., & Villagrán, C. (2005). On the persistence of tropical paleofloras in central Chile during the Early Eocene. *Review of Palaeobotany and Palynology*, *137*(1–2), 41–50. <https://doi.org/10.1016/j.revpalbo.2005.09.001>
- GBIF.org. (2021). *GBIF Home Page*. Retrieved from <https://www.gbif.org>
- Greenwood, D. R. (1987). Early Tertiary Podocarpaceae - megafossils from the Eocene Anglesea locality, Victoria, Australia. *Australian Journal of Botany*, *35*(2), 111–133. <https://doi.org/10.1071/BT9870111>
- Greenwood, D. R. (1994). Palaeobotanical evidence for Tertiary climates. In R. S. Hill (Ed.), *History of the Australian vegetation: Cretaceous to recent* (pp. 44–59). Cambridge University Press.
- Greenwood, D. R. (1996). Eocene monsoon forests in central Australia? *Australian Systematic Botany*, *9*(2), 95–112. <https://doi.org/10.1071/SB9960095>
- Greenwood, D. R. (2005). Leaf margin analysis: Taphonomic constraints. *PALAIOS*, *20*(5), 498–505. <https://doi.org/10.2110/palo.2004.P04-58>
- Greenwood, D. R. (2007). Fossil angiosperm leaves and climate: From Wolfe and Dilcher to Burnham and Wilf. In D. Jarzen, G. Retallack, S. Jarzen, & S. Manchester (Eds.), *Advances in Mesozoic and Cenozoic Paleobotany: studies in celebration of David L. Dilcher and Jack A. Wolfe* (Vol. 258, pp. 95–108). Courier Forschungsinstitut Senckenberg.
- Greenwood, D. R., & Christophel, D. C. (2005). The origins and Tertiary history of Australian “Tropical” rainforests. In E. Bermingham, C. Dick, & C. Moritz (Eds.), *Tropical rainforests: Past, present, and future* (pp. 336–373). Univ. Chicago Press.
- Greenwood, D. R., Keefe, R. L., Reichgelt, T., & Webb, J. A. (2017). Eocene paleobotanical altimetry of Victoria's eastern Uplands. *Australian Journal of Earth Sciences*, *64*(5), 625–637. <https://doi.org/10.1080/08120099.2017.1318793>
- Greenwood, D. R., Moss, P. T., Rowett, A. I., Vadala, A. J., & Keefe, R. L. (2003). *Plant Communities and Climate Change in Southeastern Australia during the Early Paleogene* (Vol. 369, pp. 365–380). Geological Society of America Special Paper. <https://doi.org/10.1130/0-8137-2369-8.365>
- Greenwood, D. R., Vadala, A. J., & Douglas, J. G. (2000). Victorian Paleogene and Neogene macrofloras: A conspectus. *Proceedings of the Royal Society of Victoria*, *112*(1), 65–92. <https://doi.org/10.1080/11035890001221065>
- Greenwood, D. R., Wilf, P., Wing, S. L., & Christophel, D. C. (2004). Paleotemperature estimation using leaf-margin analysis: Is Australia different? *PALAIOS*, *19*(2), 129–142. [https://doi.org/10.1669/0883-1351\(2004\)019<0129:PEULAI>2.0.CO;2](https://doi.org/10.1669/0883-1351(2004)019<0129:PEULAI>2.0.CO;2)
- Greenwood, D. R., & Wing, S. L. (1995). Eocene continental climates and latitudinal temperature gradients. *Geology*, *23*(11), 1044–1048. [https://doi.org/10.1130/0091-7613\(1995\)023<1044:ECCALT>2.3.CO;2](https://doi.org/10.1130/0091-7613(1995)023<1044:ECCALT>2.3.CO;2)
- Grein, M., Konrad, W., Wilde, V., Utescher, T., & Roth-Nebelsick, A. (2011). Reconstruction of atmospheric CO₂ during the early middle Eocene by application of a gas exchange model to fossil plants from the Messel Formation, Germany. *Palaeogeography, Palaeoclimatology, Palaeoecology*, *309*(3–4), 383–391. <https://doi.org/10.1016/j.palaeo.2011.07.008>
- Grimm, G. W., & Potts, A. J. (2016). Fallacies and fantasies: The theoretical underpinnings of the Coexistence Approach for palaeoclimate reconstruction. *Climate of the Past*, *12*, 611–622. <https://doi.org/10.5194/cp-12-611-2016>
- Habeck-Fardy, A., & Nanson, G. C. (2014). Environmental character and history of the Lake Eyre Basin, one seventh of the Australian continent. *Earth-Science Reviews*, *132*, 39–66. <https://doi.org/10.1016/j.earscirev.2014.02.003>
- Hagen, E. R., Royer, D. L., Moye, R. A., & Johnson, K. R. (2019). No large bias within species between the reconstructed areas of complete and fragmented fossil leaves. *PALAIOS*, *34*(1), 43–48. <https://doi.org/10.2110/palo.2018.091>
- Herold, N., Buzan, J., Seton, M., Goldner, A., Green, J. A. M., Müller, R. D., et al. (2014). A suite of early Eocene (~55 Ma) climate model boundary conditions. *Geoscientific Model Development*, *7*, 2077–2090. <https://doi.org/10.5194/gmd-7-2077-2014>
- Herold, N., Huber, M., Greenwood, D. R., Müller, R. D., & Seton, M. (2011). Early to middle Miocene monsoon climate in Australia. *Geology*, *39*(1), 3–6. <https://doi.org/10.1130/G31208.1>
- Hijmans, R. J., Cameron, S. E., Parra, J. L., Jones, P. G., & Jarvis, A. (2005). Very high resolution interpolated climate surfaces for global land areas. *International Journal of Climatology*, *25*(15), 1965–1978. <https://doi.org/10.1002/joc.1276>
- Hill, R. S. (1982). The Eocene megafossil flora of Nerriga, New South Wales, Australia. *Palaeontographica Abteilung B*, *181*(1–3), 44–77.
- Hill, R. S. (1986). Lauraceous leaves from the Eocene of Nerriga, New South Wales. *Alcheringa: An Australasian Journal of Palaeontology*, *10*(4), 327–351. <https://doi.org/10.1080/03115518608619144>
- Hinojosa, L. F. (2005). Climatic and vegetational changes inferred from Cenozoic southern South American paleoflora. *Revista Geologica de Chile*, *32*(1), 95–115. <https://doi.org/10.4067/s0716-02082005000100006>
- Hinojosa, L. F., Armesto, J. J., & Villagrán, C. (2006). Are Chilean coastal forests pre-Pleistocene relicts? Evidence from foliar physiognomy, palaeoclimate, and phytogeography. *Journal of Biogeography*, *33*(2), 331–341. <https://doi.org/10.1111/j.1365-2699.2005.01350.x>
- Hinojosa, L. F., Pesce, O., Yabe, A., Uemura, K., & Nishida, H. (2006). Physiognomical analysis and paleoclimate of the Ligorio Márquez fossil flora, Ligorio Márquez Formation, 46°45'S, Chile. In H. Nishida (Ed.), *Post-Cretaceous floristic changes in southern Patagonia, Chile* (pp. 45–55). ChuoUniv.
- Hinojosa, L. F., & Villagrán, C. (2005). Did South American Mixed Paleofloras evolve under thermal equability or in the absence of an effective Andean barrier during the Cenozoic? *Palaeogeography, Palaeoclimatology, Palaeoecology*, *217*(1–2), 1–23. <https://doi.org/10.1016/j.palaeo.2004.11.013>
- Ho, S. L., & Laepple, T. (2016). Flat meridional temperature gradient in the early Eocene in the subsurface rather than surface ocean. *Nature Geoscience*, *9*, 606–610. <https://doi.org/10.1038/ngeo2763>
- Holdgate, G. R., Wallace, M. W., Gallagher, S. J., Wagstaff, B. E., & Moore, D. (2008). No mountains to snow on: Major post-Eocene uplift of the east Victoria Highlands, evidence from Cenozoic deposits. *Australian Journal of Biological Sciences*, *55*(2), 211–234. <https://doi.org/10.1080/08120090701689373>
- Hollis, C. J., Dunkley Jones, T., Anagnostou, E., Bijl, P. K., Cramwinckel, M. J., Cui, Y., et al. (2019). The DeepMIP contribution to PMIP4: Methodologies for selection, compilation and analysis of latest Paleocene and early Eocene climate proxy data, incorporating version 0.1 of the DeepMIP database. *Geoscientific Model Development*, *12*(7), 3149–3206. <https://doi.org/10.5194/gmd-12-3149-2019>
- Huber, M., & Caballero, R. (2011). The early Eocene equable climate problem revisited. *Climate of the Past*, *7*(2), 603–633. <https://doi.org/10.5194/cp-7-603-2011>
- Hutchinson, D. K., de Boer, A. M., Coxall, H. K., Caballero, R., Nilsson, J., & Baatsen, M. (2018). Climate sensitivity and meridional overturning circulation in the late Eocene using GFDL CM2.1. *Climate of the Past*, *14*, 789–810. <https://doi.org/10.5194/cp-14-789-2018>
- Huurdeman, E. P., Frieling, J., Reichgelt, T., Bijl, P. K., Bohaty, S. M., Holdgate, G. R., et al. (2021). Rapid expansion of meso-megathermal rain forests into the southern high latitudes at the onset of the Paleocene-Eocene Thermal Maximum. *Geology*, *49*(1), 40–44. <https://doi.org/10.1130/G47343.1>
- Hyland, E. G., & Sheldon, N. D. (2013). Coupled CO₂-climate response during the early Eocene climatic optimum. *Palaeogeography, Palaeoclimatology, Palaeoecology*, *369*, 125–135. <https://doi.org/10.1016/j.palaeo.2012.10.011>

- Hyland, E. G., Sheldon, N. D., & Cotton, J. M. (2017). Constraining the early Eocene climatic optimum: A terrestrial interhemispheric comparison. *The Geological Society of America Bulletin*, 129(1–2), 244–252. <https://doi.org/10.1130/B31493.1>
- Inglis, G. N., Farnsworth, A., Lunt, D., Foster, G. L., Hollis, C. J., Pagani, M., et al. (2015). Descent toward the Icehouse: Eocene sea surface cooling inferred from GDGT distributions. *Paleoceanography*, 30(7), 1000–1020. <https://doi.org/10.1002/2014PA002723>
- Kennedy, E. M., Arens, N. C., Reichgelt, T., Spicer, R. A., Spicer, T. E. V., Stranks, L., & Yang, J. (2014). Deriving temperature estimates from Southern Hemisphere leaves. *Palaeogeography, Palaeoclimatology, Palaeoecology*, 412, 80–90. <https://doi.org/10.1016/j.palaeo.2014.07.015>
- Kershaw, A. P. (1997). A bioclimatic analysis of Early to Middle Miocene Brown coal floras, Latrobe Valley, south-eastern Australia. *Australian Journal of Botany*, 45(3), 373–387. <https://doi.org/10.1071/BT96033>
- Kiehl, J. T., Zarzycki, C. M., Shields, C. A., & Roststein, M. V. (2021). Simulated changes to tropical cyclones across the Paleocene-Eocene Thermal Maximum (PETM) boundary. *Palaeogeography, Palaeoclimatology, Palaeoecology*, 572, 110421. <https://doi.org/10.1016/j.palaeo.2021.110421>
- Kottek, M., Grieser, J., Beck, C., Rudolf, B., & Rubel, F. (2006). World map of the Köppen-Geiger climate classification updated. *Meteorologische Zeitschrift*, 15(3), 259–263. <https://doi.org/10.1127/0941-2948/2006/0130>
- Li, Y., Reich, P. B., Schmid, B., Shrestha, N., Feng, X., Lyu, T., et al. (2020). Leaf size woody dicots predicts ecosystem primary productivity. *Ecology Letters*, 23(6), 1003–1013. <https://doi.org/10.1111/ele.13503>
- Li, Y., Wang, Z., Xu, X., Han, W., Wang, Q., & Zou, D. (2016). Leaf margin analysis of Chinese woody plants and the constraints on its application to palaeoclimatic reconstruction. *Global Ecology and Biogeography*, 25(12), 1401–1415. <https://doi.org/10.1111/geb.12498>
- Little, S. A., Kembel, S. W., & Wilf, P. (2010). Paleotemperature proxies from leaf fossils reinterpreted in light of evolutionary history. *PLoS One*, 5(12), e15161. <https://doi.org/10.1371/journal.pone.0015161>
- Lowe, A. J., Greenwood, D. R., West, C. K., Galloway, J. M., Sudermann, M., & Reichgelt, T. (2018). Plant community ecology and climate on an upland volcanic landscape during the early Eocene climatic optimum: McAbee fossil beds, British Columbia, Canada. *Palaeogeography, Palaeoclimatology, Palaeoecology*, 511, 433–448. <https://doi.org/10.1016/j.palaeo.2018.09.010>
- Lunt, D. J., Bragg, F., Chan, W.-L., Hutchinson, D. K., Ladant, J.-B., Morozova, P., et al. (2021). DeepMIP: Model intercomparison of early Eocene climatic optimum (EEOC) large-scale climate features and comparison with proxy data. *Climate of the Past*, 17(1), 203–227. <https://doi.org/10.5194/cp-17-203-2021>
- Lunt, D. J., Huber, M., Anagnostou, E., Baatsen, M. L. J., Caballero, R., DeConto, R., et al. (2017). The DeepMIP contribution to PMIP4: Experimental design for model simulations of the EEOC, PETM, and pre-PETM (version 1.0). *Geoscientific Model Development*, 10(2), 889–901. <https://doi.org/10.5194/gmd-10-889-2017>
- Lusk, C. H., Clearwater, M. J., Laughlin, D. C., Harrison, S. P., Prentice, I. C., Nordenstahl, M., & Smith, B. (2018). Frost and leaf-size gradients in forests: Global patterns and experimental evidence. *New Phytologist*, 219(2), 565–573. <https://doi.org/10.1111/nph.15202>
- Macphail, M. K., Alley, N. F., Truswell, E. M., & Sluiter, I. R. K. (1994). Early Tertiary vegetation: Evidence from spores and pollen. In R. S. Hill (Ed.), *History of the Australian vegetation: Cretaceous to recent* (pp. 189–261). Cambridge University Press.
- Maechler, M., Rousseeuw, P., Struyf, A., Hubert, M., & Hornik, K. (2021). *Cluster: Cluster analysis basics and extensions*. R package.version 2.1.2.
- Moreira Rios, A. B., de Oliveira Menino, G. C., & Casagrande Dalvi, V. (2020). Leaf teeth in eudicots: What can anatomy elucidate? *Botanical Journal of the Linnean Society*, 193(4), 504–522. <https://doi.org/10.1093/botlinnean/boaa028>
- Morton, S. R., Stafford Smith, D. M., Dickman, C. R., Dunkerley, D. L., Friedel, M. H., McAllister, R. R. J., et al. (2011). A fresh framework for the ecology of arid Australia. *Journal of Arid Environments*, 75(4), 313–329. <https://doi.org/10.1016/j.jaridenv.2010.11.001>
- Naafs, B. D. A., Rohrsen, M., Inglis, G. N., Lähteenoja, O., Feakins, S. J., Collinson, M. E., et al. (2018). High temperatures in the terrestrial mid-latitudes during the early Palaeogene. *Nature Geoscience*, 11, 766–771. <https://doi.org/10.1038/s41561-018-0199-0>
- Oskanen, J., Guillaume Blanchet, F., Friendly, M., Kindt, R., Legendre, P., McGlinn, et al. (2019). *vegan: Community Ecology Package*. R package version 2 (pp. 5–6).
- Pagani, M., Huber, M., Liu, Z., Bohaty, S. M., Henderiks, J., Sijp, W., et al. (2011). The role of carbon dioxide during the onset of Antarctic glaciation. *Science*, 334(6060), 1261–1264. <https://doi.org/10.1126/science.1203909>
- Pagani, M., Zachos, J. C., Freeman, K. H., Tipple, B., & Bohaty, S. (2005). Marked decline in atmospheric carbon dioxide concentrations during the Paleogene. *Science*, 309(5734), 600–603. <https://doi.org/10.1126/science.1110063>
- Pancost, R. D., Taylor, K. W. R., Inglis, G. N., Kennedy, E. M., Handley, L., Hollis, C. J., et al. (2013). Early Paleogene evolution of terrestrial climate in the SW Pacific, Southern New Zealand. *Geochemistry, Geophysics, Geosystems*, 14(12), 5413–5429. <https://doi.org/10.1002/2013GC004935>
- Parkhurst, D. F., & Loucks, O. L. (1972). Optimal leaf size in relation to environment. *Journal of Ecology*, 60(2), 505–537. <https://doi.org/10.2307/2258359>
- Pearson, P. N., & Palmer, M. R. (2000). Atmospheric carbon dioxide concentrations over the past 60 million years. *Nature*, 406, 695–699. <https://doi.org/10.1038/35021000>
- Peppe, D. J., Baumgartner, A., Flynn, A., & Blonder, B. (2018). Reconstructing paleoclimate and paleoecology using fossil leaves. In D. A. Croft, D. F. Su, & S. W. Simpson (Eds.), *Methods in paleoecology. Vertebrate paleobiology and paleoanthropology* (pp. 289–317). Springer. https://doi.org/10.1007/978-3-319-94265-0_13
- Peppe, D. J., Royer, D. L., Cariolino, B., Oliver, S. Y., Newman, S., Leight, E., et al. (2011). Sensitivity of leaf size and shape to climate: Global patterns and paleoclimatic applications. *New Phytologist*, 190(3), 724–739. <https://doi.org/10.1111/j.1469-8137.2010.03615.x>
- Pole, M. S. (2007). Early Eocene dispersed cuticles and mangrove to rainforest vegetation at Strahan-Regatta Point, Tasmania. *Palaeontologia Electronica*, 10(3), 66. Retrieved from http://palaeo-electronica.org/2007_3/126/index.html
- Pole, M. S. (2019). *Early Eocene Plant Macrofossils from the Booval Basin, Dinmore, Near Brisbane, Queensland* (Vol. 22, pp. 1–33). Palaeontologia Electronica. <https://doi.org/10.26879/922.3.60>
- Pole, M. S., & Macphail, M. K. (1996). Eocene *Nypa* from Regatta point, Tasmania. *Review of Palaeobotany and Palynology*, 92(1–2), 55–67. [https://doi.org/10.1016/0034-6667\(95\)00099-2](https://doi.org/10.1016/0034-6667(95)00099-2)
- Pross, J., Contreras, L., Bijl, P. K., Greenwood, D. R., Bohaty, S. M., Schouten, S., et al. (2012). Persistent near-tropical warmth on the Antarctic continent during the early Eocene epoch. *Nature*, 488, 73–77. <https://doi.org/10.1038/nature11300>
- Punyasena, S. W. (2008). Estimating Neotropical palaeotemperature and palaeoprecipitation using plant family climatic optima. *Palaeogeography, Palaeoclimatology, Palaeoecology*, 265(3–4), 226–237. <https://doi.org/10.1016/j.palaeo.2008.04.025>
- R Core Team. (2020). *R: A language and environment for statistical computing*. R Foundation for Statistical Computing. Retrieved from <https://www.R-project.org/>

- Reichgelt, T., D'Andrea, W. J., Valdivia-McCarthy, A. d. C., Fox, B. R. S., Bannister, J. M., Conran, J. G., et al. (2020). Elevated CO₂, increased leaf-level productivity, and water-use efficiency during the early Miocene. *Climate of the Past*, 16(4), 1509–1521. <https://doi.org/10.5194/cp-16-1509-2020>
- Reichgelt, T., Greenwood, D. R., Steinig, S., Conran, J. G., Hutchinson, D. K., Lunt, D. J., et al. (2022). *Data supplement to: Plant proxy evidence for high rainfall and productivity in the Eocene of Australia*. Dryad. <https://doi.org/10.5061/dryad.59zw3r294>
- Reichgelt, T., Kennedy, E. M., Conran, J. G., Lee, W. G., & Lee, D. E. (2019). The presence of moisture deficits in Miocene New Zealand. *Global and Planetary Change*, 172, 268–277. <https://doi.org/10.1016/j.gloplacha.2018.10.013>
- Reichgelt, T., Kennedy, E. M., Conran, J. G., Mildenhall, D. C., & Lee, D. E. (2015). The early Miocene paleolake Manuherikia: Vegetation heterogeneity and warm-temperate to subtropical climate in southern New Zealand. *Journal of Paleolimnology*, 53, 349–365. <https://doi.org/10.1007/s10933-015-9827-5>
- Reichgelt, T., & Lee, W. G. (2021). Geographic variation of leaf form among indigenous woody angiosperms in New Zealand. *New Zealand Journal of Botany*. <https://doi.org/10.1080/0028825X.2021.1960384>
- Reichgelt, T., West, C. K., & Greenwood, D. R. (2018). The relation between global palm distribution and climate. *Scientific Reports*, 8, 4721. <https://doi.org/10.1038/s41598-018-23147-2>
- Retallack, G. J. (2009). Greenhouse crises of the past 300 million years. *The Geological Society of America Bulletin*, 121(9–10), 1441–1455. <https://doi.org/10.1130/B26341.1>
- Royer, D. L., Kooyman, R. M., Little, S. A., & Wilf, P. (2009). Ecology of leaf teeth: A multi-site analysis from an Australia subtropical rainforest. *American Journal of Botany*, 96(4), 738–750. <https://doi.org/10.3732/ajb.0800282>
- Royer, D. L., & Wilf, P. (2006). Why do toothed leaves correlate with cold climates? Gas exchange at leaf margins provide new insights into a classic paleotemperature proxy. *International Journal of Plant Sciences*, 167(1), 11–18. <https://doi.org/10.1086/497995>
- Rozefelds, A. C., Dettman, M. E., Clifford, H. T., & Lewis, D. (2016). Macrofossil evidence of early sporophyte stages of a new genus of water fern *Tecaropteris* (Ceratopteridoideae: Pteridaceae) from the Paleogene Redbank Plains Formation, southeast Queensland, Australia. *Alcheringa: An Australasian Journal of Palaeontology*, 40(1), 1–11. <https://doi.org/10.1080/03115518.2015.1069460>
- Rozefelds, A. C., Stull, G., Hayes, P., & Greenwood, D. R. (2021). The fossil record of Icacinaceae in Australia supports long-standing Palaeo-Antarctic rainforest connections in southern high latitudes. *Historical Biology*, 33(11), 2854–2864. <https://doi.org/10.1080/08912963.2020.1832089>
- Running, S., Mu, Q., & Zhao, M. (2015). MOD17A3H MODIS/Terra Net Primary Production Yearly L4 global 500m SIN Grid V006. NASA EOSDIS Land Processes DAAC. <https://doi.org/10.5067/MODIS/MOD17A3H.006>
- Scotese, C. R. (2016). *PALEOMAP PaleoAtlas for GPlates and the PaleoData plotter Program*. PALEOMAP Project.
- Scriven, L. J. (1993). Diversity of the mid-Eocene Maslin Bay flora, south Australia (Doctoral dissertation). *Adelaide research & Scholarship*. Adelaide. Retrieved from <https://hdl.handle.net/2440/21420>
- Scriven, L. J., & Hill, R. S. (1995). Macrofossil Casuarinaceae: Their identification and the oldest macrofossil record, *Gymnostoma antiquum* sp. nov., from the late Paleocene of New South Wales, Australia. *Australian Systematic Botany*, 8(6), 1035–1053. <https://doi.org/10.1071/SB9951035>
- Scriven, L. J., McLoughlin, S., & Hill, R. S. (1995). *Nothofagus plicata* (Nothofagaceae), a new deciduous Eocene macrofossil species, from southern continental Australia. *Review of Palaeobotany and Palynology*, 86(3–4), 199–209. [https://doi.org/10.1016/0034-6667\(94\)00145-A](https://doi.org/10.1016/0034-6667(94)00145-A)
- Shields, C. A., Kiehl, J. T., Rush, W., Rothstein, M., & Snyder, M. A. (2021). Atmospheric rivers in high-resolution simulations of the Paleocene Eocene thermal maximum (PETM). *Palaeogeography, Palaeoclimatology, Palaeoecology*, 567, 110293. Article. <https://doi.org/10.1016/j.palaeo.2021.110293>
- Shukla, A., Mehrotra, R. C., Spicer, R. A., Spicer, T. E. V., & Kumar, M. (2014). Cool equatorial terrestrial temperatures and the south Asian monsoon in the early Eocene: Evidence from the Gurha mine, Rajasthan, India. *Palaeogeography, Palaeoclimatology, Palaeoecology*, 412, 187–198. <https://doi.org/10.1016/j.palaeo.2014.08.004>
- Spicer, R. A., Bera, S., De Bera, S., Spicer, T. E. V., Srivastava, G., Mehrotra, R., et al. (2011). Why do foliar physiognomic climate estimates sometimes differ from those observed? Insights from taphonomic information loss and a CLAMP case study from the Ganges Delta. *Palaeogeography, Palaeoclimatology, Palaeoecology*, 302(3–4), 381–395. <https://doi.org/10.1016/j.palaeo.2011.01.024>
- Spicer, R. A., Herman, A. B., & Kennedy, E. M. (2005). The sensitivity of CLAMP to taphonomic loss of foliar physiognomic characters. *PALAIOS*, 20(5), 429–438. <https://doi.org/10.2110/palo.2004.P04-63>
- Spicer, R. A., Herman, A. B., Liao, W., Spicer, T. E. V., Kodrul, T. M., Yang, J., & Jin, J. (2014). Cool tropics in the middle Eocene: Evidence from the Changchang flora, Hainan Island, China. *Palaeogeography, Palaeoclimatology, Palaeoecology*, 412, 1–16. <https://doi.org/10.1016/j.palaeo.2014.07.011>
- Spicer, R. A., Yang, J., Herman, A. B., Kodrul, T., Maslova, N., Spicer, T. E. V., et al. (2016). Asian Eocene monsoons as revealed by leaf architectural signatures. *Earth and Planetary Science Letters*, 449, 61–68. <https://doi.org/10.1016/j.epsl.2016.05.036>
- Spicer, R. A., Yang, J., Spicer, T. E. V., & Farnsworth, A. (2021). Woody dicot leaf traits as a palaeoclimate proxy: 100 years of development and application. *Palaeogeography, Palaeoclimatology, Palaeoecology*, 562, 110138. <https://doi.org/10.1016/j.palaeo.2020.110138>
- Steinthorsdottir, M., Vajda, V., Pole, M., & Holdgate, G. (2019). Moderate levels of Eocene pCO₂ indicated by Southern Hemisphere fossil plant stomata. *Geology*, 47(10), 914–918. <https://doi.org/10.1130/G46274.1>
- Sullivan, A., McCaw, L., Gomes Da Cruz, M., Matthews, S., & Ellis, P. (2012). Fuel, fire weather and fire behaviour in Australian ecosystems. In R. A. Bradstock, A. M. Gill, & R. J. Williams (Eds.), *Flammable Australia: Fire regimes, Biodiversity and ecosystems in a changing world* (pp. 51–77). CSIRO Publishing. Retrieved from <http://hdl.handle.net/102.100.100/101433?index=1>
- Teodoridis, V., Kvaček, Z., Zhu, H., & Mazouch, P. (2012). Environmental analysis of the mid-latitude European Eocene sites of plant macrofossils and their possible analogues in East Asia. *Palaeogeography, Palaeoclimatology, Palaeoecology*, 333–334, 40–58. <https://doi.org/10.1016/j.palaeo.2012.03.008>
- Tian, Y., Dickinson, R. E., Zhou, L., Zeng, X., Dai, Y., Myneni, R. B., et al. (2004). Comparison of seasonal and spatial variations of leaf area index and fraction of absorbed photosynthetically active radiation from Moderate Resolution Imaging Spectroradiometer (MODIS) and Common Land Model. *Journal of Geophysical Research*, 109(D1), D01103. <https://doi.org/10.1029/2003JD003777>
- Truswell, E. M. (1993). Vegetation in the Australian Tertiary in response to climatic and phytogeographic forcing factors. *Australian Systematic Botany*, 6(6), 533–557. <https://doi.org/10.1071/SB9930533>
- Utescher, T., Bruch, A. A., Erdei, B., François, L., Ivanov, D., Jacques, F. M. B., et al. (2014). The Coexistence Approach—Theoretical background and practical considerations of using plant fossils for climate quantification. *Palaeogeography, Palaeoclimatology, Palaeoecology*, 410, 58–73. <https://doi.org/10.1016/j.palaeo.2014.05.031>

- Vadala, A. J., & Greenwood, D. R. (2001). Australian Paleogene vegetation and environments: Evidence for palaeo-Gondwanan elements in the fossil records of Lauraceae and Proteaceae. In I. Metcalfe, J. M. B. Smith, M. Morwood, & I. Davidson (Eds.), *Faunal and floral migration and evolution in SE Asia-Australasia* (pp. 201–226). Swets & Zeitlinger.
- Ward, J. H., Jr. (1963). Hierarchical grouping to optimize an objective function. *Journal of the American Statistical Association*, 58(301), 236–244. <https://doi.org/10.1080/01621459.1963.10500845>
- Webb, L. J. (1968). Environmental relationships of the structural types of Australian rain forest vegetation. *Ecology*, 49(2), 296–311. <https://doi.org/10.2307/1934459>
- Westerhold, T., Marwan, N., Drury, A. J., Liebrand, D., Agnini, C., Anagnostou, E., et al. (2020). An astronomically dated record of Earth's climate and its predictability over the last 66 million years. *Science*, 369(6509), 1383–1387. <https://doi.org/10.1126/science.aba6853>
- West, C. K., Greenwood, D. R., Reichgelt, T., Lowe, A. J., Vachon, J. M., & Basinger, J. F. (2020). Paleobotanical proxies for early Eocene climates and ecosystems in northern North America from middle to high latitudes. *Climate of the Past*, 16(4), 1387–1410. <https://doi.org/10.5194/cp-16-1387-2020>
- West, C. K., Reichgelt, T., & Basinger, J. F. (2021). The Ravenscrag Butte flora: Paleoclimate and paleoecology of an early Paleocene (Danian) warm-temperate deciduous forest near the vanishing inland Cannonball Seaway. *Palaeogeography, Palaeoclimatology, Palaeoecology*, 576, 110488. <https://doi.org/10.1016/j.palaeo.2021.110488>
- Weston, P. H., & Jordan, G. J. (2017). Evolutionary biogeography of the Australian flora in the Cenozoic era. In D. A. Keith (Ed.), *Australian vegetation* (pp. 40–62). Cambridge University Press.
- Whittaker, R. H. (1962). Classification of natural communities. *The Botanical Review*, 28, 1–239. <https://doi.org/10.1007/BF02860872>
- Wilf, P. (1997). When are leaves good thermometers? A new case for leaf margin analysis. *Paleobiology*, 23(3), 373–390. <https://doi.org/10.1017/S0094837300019746>
- Wilf, P., Johnson, K. R., Cúneo, N. R., Smith, M. E., Singer, B. S., & Gandolfo, M. A. (2005). Eocene plant diversity at Laguna del Hunco and Río Pichileufú, Patagonia, Argentina. *The American Naturalist*, 165(6), 634–650. <https://doi.org/10.1086/430055>
- Wilf, P., Wing, S. L., Greenwood, D. R., & Greenwood, C. L. (1998). Using fossil leaves as paleoprecipitation indicators: An Eocene example. *Geology*, 26(3), 203–206. [https://doi.org/10.1130/0091-7613\(1998\)026<0203:uflapi>2.3.co;2](https://doi.org/10.1130/0091-7613(1998)026<0203:uflapi>2.3.co;2)
- Willard, D. A., Donders, T. H., Reichgelt, T., Greenwood, D. R., Sangiorgi, F., Peterse, F., et al. (2019). Arctic vegetation, temperature, and hydrology during Early Eocene transient global warming events. *Global and Planetary Change*, 178, 139–152. <https://doi.org/10.1016/j.gloplacha.2019.04.012>
- Witkowski, C. R., Weijers, J. W. H., Blais, B., Schouten, S., & Sinninghe Damsté, J. S. (2018). Molecular fossils from phytoplankton reveal secular $p\text{CO}_2$ trend over the Phanerozoic. *Science Advances*, 4(11), 7. <https://doi.org/10.1126/sciadv.aat4556>
- Wolfe, J. A. (1993). A method of obtaining climatic parameters from leaf assemblages. *US Geological Survey Bulletin*, 2040, 1–71.
- Wright, I. J., Dong, N., Maire, V., Prentice, I. C., Westoby, M., Díaz, S., et al. (2017). Global climatic drivers of leaf size. *Science*, 357(6354), 917–921. <https://doi.org/10.1126/science.aal4760>
- Yang, J., Spicer, R. A., Spicer, T. E. V., Arens, N. C., Jacques, F. M. B., Su, T., et al. (2015). Leaf form–climate relationships on the global stage: An ensemble of characters. *Global Ecology and Biogeography*, 24(10), 1113–1125. <https://doi.org/10.1111/geb.12334>
- Zhou, S., Yu, B., Schwalm, C. R., Ciais, P., Zhang, Y., Fisher, J. B., et al. (2017). Response of water use efficiency to global environmental change based on output from terrestrial biosphere models. *Global Biogeochemical Cycles*, 31(11), 1639–1655. <https://doi.org/10.1002/2017GB005733>
- Zhu, J., Poulsen, C. J., & Tierney, J. E. (2019). Simulation of Eocene extreme warmth and high climate sensitivity through cloud feedbacks. *Science Advances*, 5(9), eaax1874. <https://doi.org/10.1126/sciadv.aax1874>
- Zhu, Z., Piao, S., Myneni, R. B., Huang, M., Zeng, Z., Canadell, J. G., et al. (2016). Greening of the Earth and its drivers. *Nature Climate Change*, 6, 791–795. <https://doi.org/10.1038/nclimate3004>